Rapid diagnosis of FHL3 by flow cytometric detection of intraplatelet Munc13-4 protein

Yuuki Murata,[1] Takahiro Yasumi,[1] Ryutaro Shirakawa,[2] Kazushi Izawa,[1] Hidemasa Sakai,[1] Junya Abe,[1] Naoko Tanaka,[1] Tomoki Kawai,[1] Koichi Oshima,[3-5] Megumu Saito,[3] Ryuta Nishikomori,[1] Osamu Ohara,[4,5] Eiichi Ishii,[6] Tatsutoshi Nakahata,[3] Hisanori Horiuchi,[2] and Toshio Heike[1]

[1]Department of Pediatrics, Kyoto University Graduate School of Medicine, Kyoto, Japan; [2]Department of Molecular and Cellular Biology, Institute of Development, Aging and Cancer, Tohoku University, Sendai, Japan; [3]Clinical Application Department, Center for iPS Cell Research and Application, Kyoto University, Kyoto, Japan; [4]Department of Human Genome Research, KAZUSA DNA Research Institute, Kisarazu, Japan; [5]Laboratory for Immunogenomics, Research Center for Allergy and Immunology, RIKEN, Yokohama, Japan; and [6]Department of Pediatrics, Ehime University Graduate School of Medicine, Toon, Japan

Familial hemophagocytic lymphohistiocytosis (FHL) is a potentially lethal genetic disorder of immune dysregulation that requires prompt and accurate diagnosis to initiate life-saving immunosuppressive therapy and to prepare for hematopoietic stem cell transplantation. In the present study, 85 patients with hemophagocytic lymphohistiocytosis were screened for FHL3 by Western blotting using platelets and by natural killer cell lysosomal exocytosis assay. Six of these patients were diagnosed with FHL3. In the acute disease phase requiring platelet transfusion, it was difficult to diagnose FHL3 by Western blot analysis or by lysosomal exocytosis assay. In contrast, the newly established flow cytometric analysis of intraplatelet Munc13-4 protein expression revealed bimodal populations of normal and Munc13-4–deficient platelets. These findings indicate that flow cytometric detection of intraplatelet Munc13-4 protein is a sensitive and reliable method to rapidly screen for FHL3 with a very small amount of whole blood, even in the acute phase of the disease. (*Blood*. 2011;118(5):1225-1230)

Introduction

The granule-dependent cytotoxic pathway is a major immune effector mechanism used by cytotoxic T lymphocytes (CTLs) and natural killer (NK) cells.[1] The pathway involves a series of steps, including cell activation, polarization of the lysosomal granules to the immunologic synapse, exocytosis of lytic proteins such as perforin and granzymes, and induction of apoptosis in the target cells.[2] In addition to its central role in the defense against intracellular infections and in tumor immunity, this pathway also plays an important role in the regulation of immune homeostasis. Defects in the granule-dependent cytotoxic pathway result in a catastrophic hyperinflammatory condition known as hemophagocytic lymphohistiocytosis (HLH).[1,3]

HLH is a life-threatening syndrome of immune dysregulation resulting from the uncontrolled activation and proliferation of CTLs, which leads to macrophage activation and the excessive release of inflammatory cytokines.[4,5] Clinical diagnosis of HLH is made on the basis of cardinal signs and symptoms including prolonged fever and hepatosplenomegaly, and by characteristic laboratory findings such as pancytopenia, hyperferritinemia, hypofibrinogenemia, increased levels of soluble IL-2 receptor, and low or absent NK cell activity.[5,6] HLH can be classified into primary (genetic) or secondary (acquired) forms according to the underlying etiology, although this distinction is difficult to make in clinical practice.[4,5]

Familial hemophagocytic lymphohistiocytosis (FHL) encompasses major forms of primary HLH for which mutations in the genes encoding perforin (*PRF1*; FHL2),[7] Munc13-4 (*UNC13D*; FHL3),[8] syntaxin-11 (*STX11*; FHL4),[9] and syntaxin-binding protein 2 (also known as Munc18-2) (*STXBP2*; FHL5)[10,11] have been identified to date. Perforin is a cytolytic effector that forms a pore-like structure in the target cell membrane. Munc13-4, syntaxin-11, and Munc18-2 are involved in intracellular trafficking or the fusion of cytolytic granules to the plasma membrane and the subsequent delivery of their contents into target cells.[1,12] Consequently, defective cytotoxic activity of CTLs and NK cells is one of the hallmark findings of FHL,[7,8,13-16] although NK cell activity is also decreased in some cases of secondary HLH.[15,17-20]

Prompt and accurate diagnosis of FHL is mandatory to initiate life-saving immunosuppressive therapy and to prepare for hematopoietic stem cell transplantation. Detection of perforin expression in NK cells with flow cytometry is a reliable method to screen for FHL2.[21] Another test analyzes the expression of CD107a on the surface of NK cells, which marks the release of cytolytic granules.[22] Reduced expression of CD107a implies impaired degranulation of NK cells and predicts a likelihood of FHL3.[23] However, this analysis is not available in some patients with extremely reduced NK cell numbers, such as during the acute phase of HLH.[19] In addition, NK-cell degranulation is also impaired in FHL4[24] and FHL5,[10,11] making it impossible to differentiate these disorders.

We reported previously that Munc13-4 protein is expressed in platelets and regulates the secretion of dense core granules.[25] Herein we report that Munc13-4 is expressed far more abundantly in platelets than in PBMCs. We also describe the development of a

Submitted January 10, 2011; accepted May 23, 2011. Prepublished online as *Blood* First Edition paper, June 8, 2011; DOI 10.1182/blood-2011-01-329540.

The online version of this article contains a data supplement.

The publication costs of this article were defrayed in part by page charge payment. Therefore, and solely to indicate this fact, this article is hereby marked "advertisement" in accordance with 18 USC section 1734.

new method to screen for FHL3 rapidly by detecting intraplatelet Munc13-4 expression through flow cytometry.

Methods

Patients

Between January 2008 and March 2010, whole blood samples from 85 patients were screened for FHL3. The patients had been clinically diagnosed with HLH by their referring physicians and were suspected of possible FHL. Characteristics of the enrolled patients are summarized in supplemental Table 1 (available on the *Blood* Web site; see the Supplemental Materials link at the top of the online article). As a control, blood obtained from healthy adults at the time of patient sampling was shipped for screening along with the patient samples. Before the laboratory studies were performed, informed consent was obtained from the patients and their parents, in accordance with the institutional review board of Kyoto University Hospital and the Declaration of Helsinki.

Preparation of PBMCs and platelet samples

Whole blood samples treated with EDTA were centrifuged gently at 100*g* for 10 minutes, and platelets were collected from the supernatant plasma layer. Alternatively, platelets were prepared from small aliquots of blood samples by lysing red blood cells with ammonium chloride. PBMCs were obtained by Ficoll-Hypaque density gradient centrifugation from the remaining sample. $CD4^+$, $CD8^+$, $CD14^+$, $CD19^+$, and $CD45^+$ cells were separated from PBMCs using an AutoMACS Pro (Miltenyi Biotec) and magnetic bead–conjugated mAbs according to the manufacturer's instructions. Flow cytometric analysis revealed that each cell population contained > 95% $CD4^+$, $CD8^+$, $CD14^+$, $CD19^+$, and $CD45^+$ cells (data not shown).

Mutation analysis

Genomic DNA was isolated from the PBMCs of patients with defective Munc13-4 expression using standard procedures. Primers were designed for the amplification and direct DNA sequencing of the *UNC13D*-coding exons, including the adjacent intronic sequences for the identification of splice-site variants. Primer sequences are available upon request. Products were sequenced directly with an ABI3130 genetic analyzer (Applied Biosystems).

Antibodies

Rabbit polyclonal antibodies raised against the N-terminal region (residues 1-262)[25] and full-length human Munc13-4 protein were used as primary antibodies for Western blot and flow cytometric analysis, respectively. Rabbit polyclonal anti-integrin αIIb (Santa Cruz Biotechnology) and mouse polyclonal anti–β-actin (Sigma-Aldrich) antibodies were used as primary antibodies for Western blotting. The mAbs used in the flow cytometric analysis were FITC-conjugated anti-CD3 (SK7; BD Pharmingen), phycoerythrin (PE)–conjugated anti-CD41a (HIP8; BD Pharmingen); allophycocyanin-conjugated anti-CD56 (N901; Beckman Coulter), and PE-conjugated anti-CD107a (H4A3; eBioscience).

Western blot analysis

Cell extracts were fractionated by SDS-PAGE, and the fractionated proteins were electrotransferred onto polyvinylidene fluoride membranes. The membranes were blocked overnight in blocking buffer (5% skim milk) and incubated for 1 hour at room temperature with the primary antibodies, followed by HRP-conjugated anti–rabbit or anti–mouse IgG polyclonal antibodies (Santa Cruz Biotechnology). Specific bands were visualized by the standard enhanced chemiluminescence method.

Flow cytometric analysis of Munc13-4 protein

After surface staining with anti-CD41a mAbs, platelets were fixed and permeabilized by Cytofix/Cytoperm (BD Biosciences) and washed 3 times with Perm/Wash buffer (BD Biosciences). After nonspecific reactions were blocked with Chrome-Pure human IgG (Jackson ImmunoResearch Laboratories), rabbit polyclonal antibody against the full-length human Munc13-4 protein was added, followed by FITC-conjugated donkey anti–rabbit IgG (Jackson ImmunoResearch Laboratories). Platelets were gated on the basis of their appearance on forward- and side-scatter plots in log/log scale and by CD41a expression. The gated platelets were analyzed for Munc13-4 expression by flow cytometry (FACSCalibur; BD Biosciences).

Lysosomal degranulation assays

To quantify lysosome exocytosis by NK cells, 2×10^5 PBMCs were mixed with 2×10^5 human erythroleukemia cell line K562 cells and incubated for 2 hours in complete medium (RPMI 1640 medium supplemented with 2mM L-glutamine and 10% FCS) at 37°C in 5% CO_2. Cells were resuspended in PBS supplemented with 2% FCS and 2mM EDTA; stained with anti-CD3–FITC, anti-CD56–allophycocyanin, and anti-CD107a–PE mAbs; and analyzed by flow cytometry.

Platelet exocytosis of the lysosomal granules was analyzed as described previously[26] but with a minor modification. Briefly, platelets were suspended in PBS containing 2mM EDTA and PE-conjugated anti-CD107a mAb, stimulated with 5 U/mL of thrombin (Wako Pure Chemical Industries) for 10 minutes at 25°C, and immediately analyzed by flow cytometry. The degranulation index of platelets was calculated as: (mean fluorescence value of stimulated sample − mean fluorescence value of nonstimulated sample)/mean fluorescence value of nonstimulated sample.

Statistical analysis

Statistical analyses were performed with 1-way ANOVA followed by the Tukey post hoc test to compare multiple groups, with a $P < .05$ level considered to be significant.

Results

Diagnosis of FHL3 by Western blot analysis using platelets

Before screening for FHL3, the Munc13-4 expression level was compared between platelets and PBMCs. Munc13-4 expression in platelets was approximately 10 times higher than that in PBMCs (Figure 1A). $CD8^+$ cells expressed a similar level of Munc13-4 protein as other PBMC cell types (Figure 1B). Similar amounts of platelet- and PBMC-derived proteins could be obtained from a sample (data not shown). Therefore, platelets were used to perform Western blotting to screen for Munc13-4 deficiency. Of the 85 patients screened, 6 patients were diagnosed with FHL3 (Figure 1C). Munc13-4 protein was barely detected in the platelets of each FHL3 patient regardless of the gene mutation (Table 1). For each sample, no more than 1 mL of whole blood was required to perform the analysis.

Difficulty in diagnosing FHL3 in the acute phase of the disease

Patients in the acute phase of the disease who require screening for FHL often receive platelet transfusions because of thrombocytopenia.[4-6] To study the effect of transfused platelets on screening results, FHL3 screening was attempted in a patient receiving platelet transfusions. As expected, Western blotting using platelets could not detect Munc13-4 deficiency because of the normal expression of the protein in the transfused platelets (Figure 2A left column). Surprisingly, Western blotting using PBMCs also could not clearly identify Munc13-4 deficiency because a substantial number of platelets were present in the PBMCs obtained by the standard method (Figure 2A right column). By positively selecting $CD45^+$ cells and removing platelets, it was found that a considerable amount of the Munc13-4 protein detected in PBMC samples

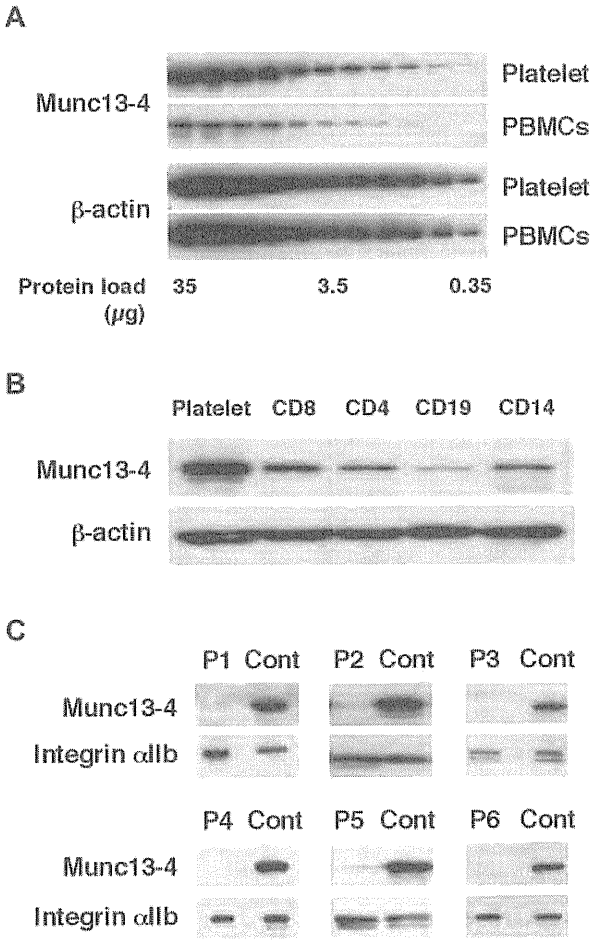

Figure 1. Diagnosing FHL3 by Western blotting using platelet protein. The amount of Munc13-4 protein expression was compared between platelets and PBMCs (A) and among platelets, $CD8^+$, $CD4^+$, $CD19^+$, and $CD14^+$ cells (B) by Western blotting. A representative result of 5 independent experiments is shown. (C) Six FHL3 patients were diagnosed by Western blotting for Munc13-4 protein using platelets.

obtained by standard density gradient centrifugation was actually derived from the contaminating platelets (Figure 2B).

We performed a NK-cell degranulation assay for every referred sample and found the assay to be defective for every FHL3 patient identified (data not shown). All of the other patients showed a normal release of lysosomal granules by NK cells; however, the analysis could not be performed in some patients because of the extremely low NK-cell number during the acute phase of the disease (data not shown).

We also examined the lysosomal granule release of platelets in 31 patients to determine whether this assay could be used as a screening method for FHL3. Lysosomal exocytosis of FHL3 platelets was partially impaired at steady state, but profound impairment was observed during the acute phase of the disease (Figure 3A-C). This profound impairment was also observed in platelets obtained from some secondary HLH patients during the acute phase (Figure 3B-C). These results indicate that it is difficult to diagnose FHL3 during the acute phase of HLH either by Western blot or by lysosomal degranulation assay.

Table 1. UNC13D gene mutations of FHL3 patients

Patient	Age at onset	Gender	Mutation	Genotype	Predicted effect
P1	14 days	Female	c.1596 + 1G → C	Homo	Splice error
P2	2 months	Male	c.322–1G → A	Hetero	Splice error
			c.990G → C	Hetero	p.Q330H
			c.3193C → T	Hetero	p.R1065X
P3	12 months	Female	c.754–1G → C	Hetero	Splice error
			c.2485delC	Hetero	p.L829fs
P4	4 months	Female	c.754–1G → C	Hetero	Splice error
			c.1799C → T	Hetero	p.T600M
			c.1803C → A	Hetero	p.Y601X
P5	2 months	Female	c.754–1G → C	Hetero	Splice error
			c.1596 + 1G → C	Hetero	Splice error
P6	5 months	Male	ND	ND	ND

Mutations were checked for single nucleotide polymorphisms using the dbSNP Build 132 database from the National Center for Biotechnology Information.

X indicates stop; fs, frame shift; and ND, not determined.

Rapid diagnosis of FHL3 by flow cytometric detection of intraplatelet Munc13-4

To overcome the difficulty in diagnosing FHL3 during the acute phase of HLH, antibodies were raised against the full-length human Munc13-4 protein (supplemental Figure 1) and a new method was developed to detect Munc13-4 protein in platelets by flow cytometry. A total of 35 patients, including 4 with FHL3 (P3-P6), were

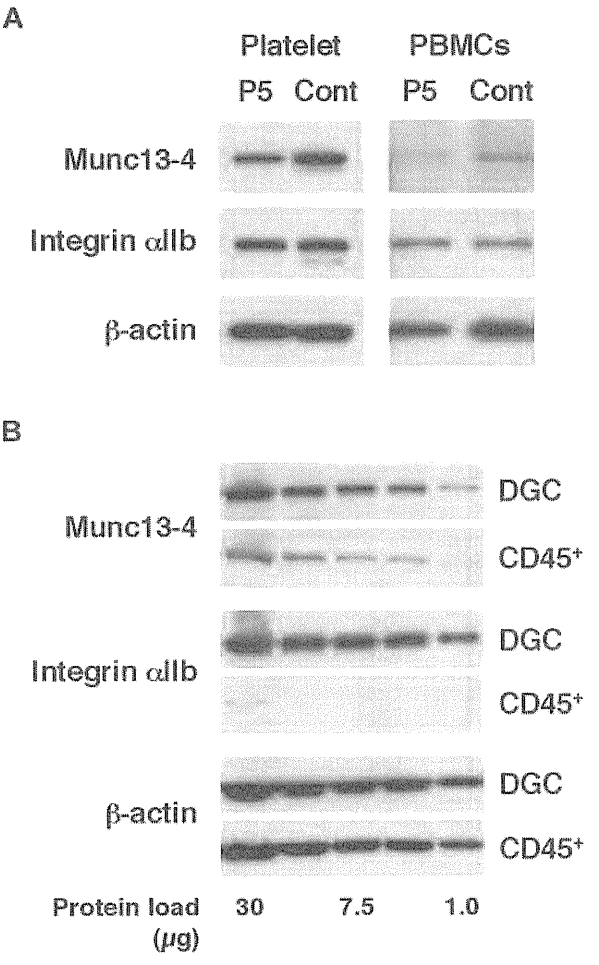

Figure 2. Effect of platelet transfusion on Western blot analysis. (A) Western blotting analysis for Munc13-4 expression using platelets and PBMCs from an FHL3 patient (P5) receiving platelet transfusions during the acute phase of the disease. (B) The expression of Munc13-4 was compared between PBMCs obtained by density gradient centrifugation (DGC) and $CD45^+$ cells obtained by magnetic sorting from healthy controls. A representative result of 3 independent experiments is shown.

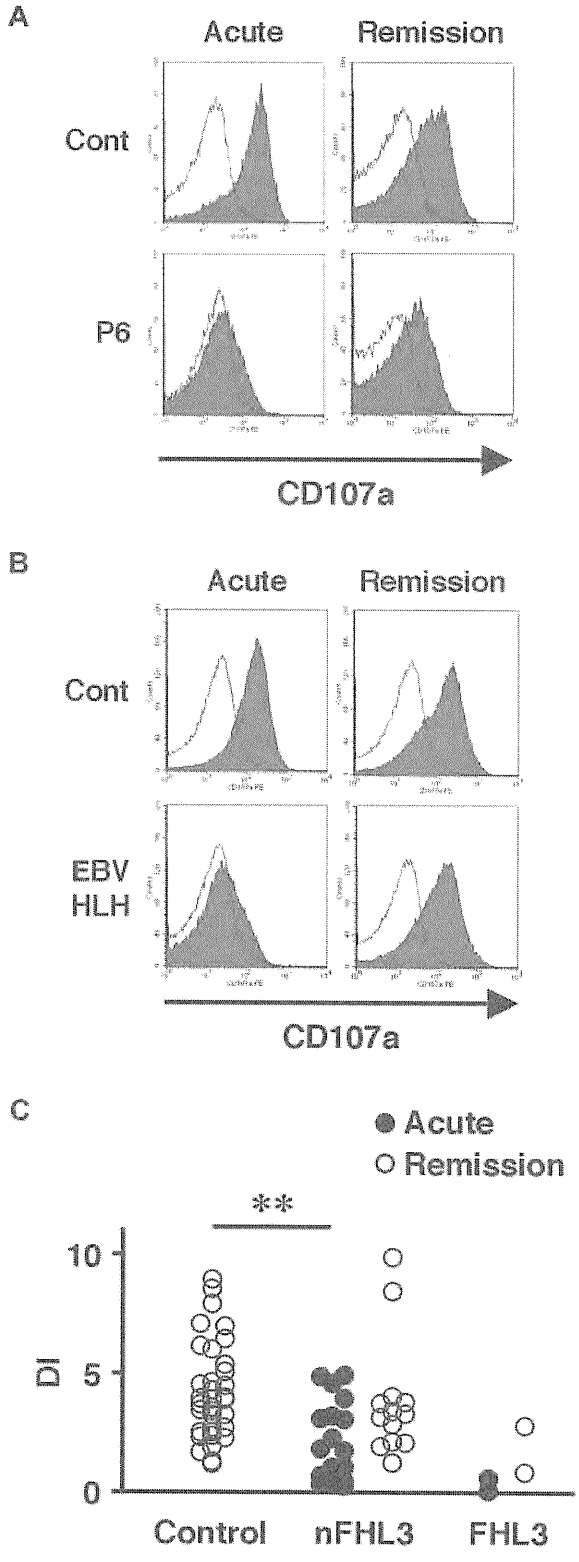

Figure 3. Analysis of lysosomal exocytosis using platelets from HLH patients. Platelets from an FHL3 patient (P6; A) and from a secondary (EBV-associated) HLH patient (B) along with healthy controls were left untreated (open histogram) or were stimulated with thrombin (closed histograms), and the surface expression of CD107a was analyzed by flow cytometry. Analysis was performed during the acute phase of the disease (left column) and after clinical remission (right column). (C) Degranulation index (DI) of platelets from HLH patients during the acute phase (●) and after clinical remission (○). HLH patients with normal NK-cell degranulation and Munc13-4 protein expression by Western blot analysis were defined as non-FHL3 (nFHL3). $^{**}P < .01$ by the Tukey post hoc test.

analyzed using this method. Munc13-4 deficiency was readily detected in all of the FHL3 patients, with a sample volume of < 100 μL of whole blood (Figure 4A-C). Munc13-4 protein was expressed at normal level in the platelets of parents and siblings of FHL3 patients carrying heterozygous *UNC13D* mutations (data not shown). In the FHL3 patient receiving platelet transfusions, flow cytometric analysis revealed bimodal populations of normal and Munc13-4–deficient platelets (P5 in Figure 4A). As shown in Figure 4B, the method was able to clearly identify Munc13-4–deficient platelets in whole blood samples stored at room temperature for 1 week.

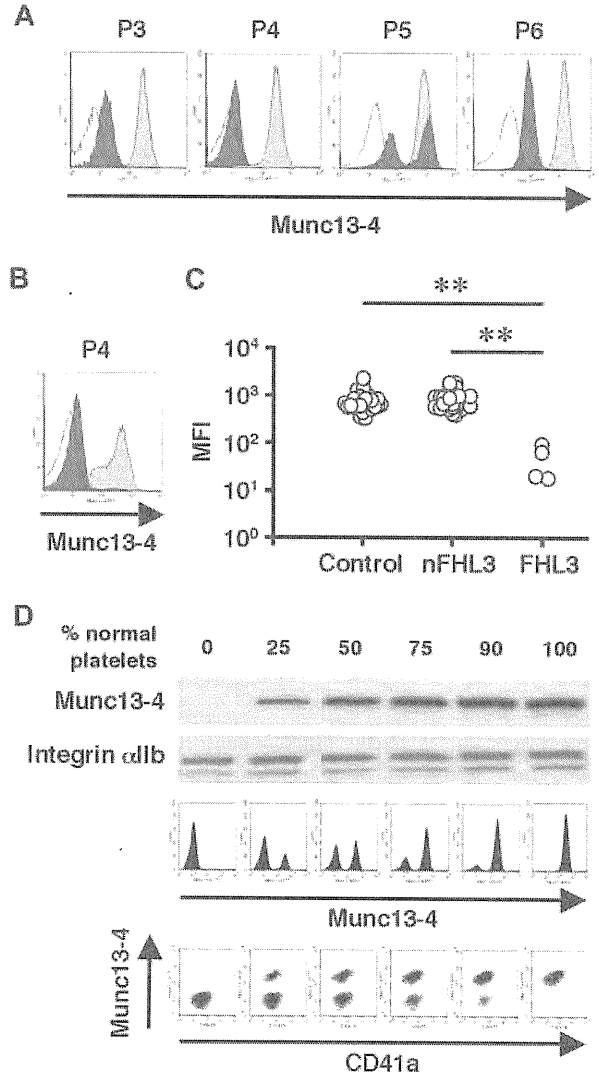

Figure 4. Flow cytometric detection of intraplatelet Munc13-4 protein. Flow cytometric analysis of intraplatelet Munc13-4 expression in 4 FHL3 patients and healthy controls using whole blood samples shipped overnight (A) and in an FHL3 patient (P4) and a healthy control using samples stored at room temperature for a week (B). Dark closed histograms represent platelets from FHL3 patients, whereas light closed histograms represent platelets from healthy controls. Open histograms represent staining with isotype controls. (C) Mean fluorescence intensity (MFI) of intraplatelet Munc13-4 staining for HLH patients and healthy controls. All of the healthy controls (n = 35) were adults. Non-FHL3 (nFHL3) patients (n = 31), as defined in Figure 3, varied in age (2 days-39 years) and included 2 patients with FHL2. Age-related variations in the MFI of Munc13-4 staining were not observed. $^{**}P < .01$ by the Tukey post hoc test. (D) The sensitivities of Western blot and flow cytometric analyses for detecting Munc13-4–deficient platelets were compared.

To determine the sensitivity of the new method, Munc13-4–deficient platelets were mixed with normal platelets at varying ratios. Western blot analysis could not detect Munc13-4–deficient platelets easily, even when the proportion of normal platelets was as low as 25% (Figure 4D). In contrast, flow cytometric analysis easily identified 10% Munc13-4–deficient platelets among 90% normal platelets (Figure 4D), which proved the high sensitivity of the method in diagnosing FHL3.

Discussion

FHL is a rare but life-threatening inherited immune disorder for which mutations in 4 genes have been identified as causative factors. *PRF1* encodes the cytolytic effector protein perforin that forms a pore-like structure in the target cell membrane.[1,12] A mutation in *PRF1* results in FHL2,[7] which accounts for 20%-50% of FHL cases.[4,5] *UNC13D* encodes the protein Munc13-4, which is crucial for the fusion of cytolytic granules to the plasma membrane and the subsequent release of perforin and granzymes.[1,12] Mutations in *UNC13D* result in FHL3,[8] which accounts for 20%-30% of FHL cases.[4,12] FHL4 is caused by mutations in *STX11*, which encodes syntaxin-11.[9] Mutations in *STXBP2*, which encodes Munc18-2, were recently reported to cause FHL5.[10,11] Syntaxin-11 and Munc18-2 also mediate the fusion of cytolytic granules to the plasma membrane.[1,5,12] The ability to screen for FHL2-5 rapidly would facilitate the initiation of life-saving immunosuppressive therapy and the preparation of FHL patients for hematopoietic stem cell transplantation.

In the present study, we found that the Munc13-4 protein is expressed abundantly in platelets (Figure 1A-B). The detection of Munc13-4 protein in platelets by Western blotting (Figure 1C) or flow cytometry (Figure 4A-B) was a reliable screening method to identify FHL3 patients. Munc13-4–deficient platelets were identified easily among normal transfused platelets by flow cytometry, which indicated that this method could be applied to patients who are receiving platelet transfusions during the acute phase of the disease (P5 in Figure 4A). Detection of intraplatelet Munc13-4 was enabled by the use of highly specific antibodies against the full-length human Munc13-4 (supplemental Figure 1).

There is a possibility that FHL3 patients with residual Munc13-4 protein expression could be overlooked by the screening methods described in this study. Most FHL3 patients have mutations that result in the absence or significant reduction of Munc13-4 protein expression,[16,23] as was the case with the patients screened in this study (Figure 1C), which suggests that the mutated Munc13-4 protein is unstable. The NK-cell degranulation assay, which was performed for every referred sample with a sufficient number of NK cells, revealed defective degranulation only in the identified FHL3 patients (date not shown). These results indicate that the majority of mutations in *UNC13D* are likely amenable to rapid detection by the new methods described in this study. Comparative studies on the *UNC13D* genotype, Munc13-4 protein expression, and the lysosomal exocytosis assay must be performed to confirm the reliability of these methods.

It was also investigated whether the analysis of lysosomal release by platelets could be used as an alternative method to screen for FHL3. Profound impairment of lysosomal exocytosis by platelets during the acute phase of the disease and restoration of this impairment after clinical remission was observed in FHL3 and in some secondary HLH patients (Figure 3). It is not clear whether this transient impairment of platelet degranulation is involved in HLH pathogenesis or if it merely reflects in vivo platelet activation by diffuse endothelial damage during the acute phase of the disease that renders them unresponsive to ex vivo stimulation. The release of lysosomal granules by Munc13-4–deficient platelets was impaired only minimally at steady state (Figure 3A and 3C), which is in contrast to a recent study showing the involvement of the Munc13-4 protein in the release of lysosomal granules in mouse platelets.[27] Although the precise reason for this discrepancy is unclear, platelet degranulation is likely to be regulated differentially between species; for example, Munc13-4–deficient mice have bruising and bleeding tendencies[27] that are not commonly associated with human FHL3. Further studies are warranted to elucidate the exocytosis pathways of platelets and their role in the pathophysiology of HLH.

With the development of tools for rapid screening, the diagnostic approach for FHL has changed over the years. Impaired NK cytotoxicity was the first reported signature clinical finding of FHL patients.[13,14] Defective CTL activity was subsequently reported as another hallmark of FHL.[7,8,16,28] However, NK-cell activity is also decreased in some cases of secondary HLH,[15,17-20] and the CTL cytotoxicity assay is not readily accessible to most clinicians. The NK-cell lysosomal exocytosis assay is a comprehensive method to identify patients with a degranulation defect.[10,11,22-24] However, this analysis is not available in some patients with extremely reduced NK-cell numbers, which are often observed during the acute phase of HLH.[19] Although CTLs can be an alternative tool to perform the lysosomal exocytosis assay,[24,28,29] it remains impossible to differentiate FHL3-FHL5.[10,11,23,24] Impairment in these assays warrants the genetic confirmation of FHL, but sequencing all of the candidate genes is not a suitable approach for rapid diagnosis. Flow cytometric detection of perforin expression in NK cells is a reliable and rapid way of identifying patients with FHL2,[21] and the new method described in this study for the detection of Munc13-4 expression in platelets would add to the rapid diagnosis of FHL3.

Platelets could also be used for the screening of FHL4 and FHL5 because they share some granule-transport mechanisms with other types of hematopoietic cells, including CTLs and NK cells.[2,30,31] Indeed, in the present study, both syntaxin-11 and Munc18-2 were expressed abundantly in platelets (data not shown). We are currently using platelet proteins to screen for FHL4-FHL5 by Western blot analysis, although no cases have been found so far because of the extreme rarity of these disorders.

In summary, platelets abundantly express Munc13-4 protein and are a useful tool to screen for FHL3. By detecting intraplatelet Munc13-4 expression by flow cytometry, it is now possible to rapidly screen for FHL3 with a very small sample of whole blood, even in the acute disease phase requiring platelet transfusion. Because platelets share some of their granule transport systems with other types of hematopoietic cells, they could also be used to screen for other types of immune disorders, including FHL4 and FHL5.

Acknowledgments

The authors are grateful to all of the participating patients, their families, and the referring physicians for their generous cooperation in this study.

This study was supported by grants from The Morinaga Foundation for Health and Nutrition; from the Japanese Ministry of

Education, Culture, Sports, Science, and Technology; and from the Japanese Ministry of Health, Labor, and Welfare.

Authorship

Contribution: T.Y., R.N., T.N., H.H., and H.T. designed the research; Y.M., K.I., and M.S. performed the Western blot and flow cytometric analyses; K.O. and O.O. performed the genetic analyses; R.S. and H.H. prepared the anti–Munc13-4 antibodies and started the FHL3 screening; Y.M., T.Y., R.S., K.I., H.S., J.A., N.T., T.K., R.N., E.I., T.N., H.H., and T.H. analyzed and discussed the results; and Y.M., T.Y., and T.H. wrote the manuscript.

Conflict-of-interest disclosure: The authors declare no competing financial interests.

Correspondence: Takahiro Yasumi, Department of Pediatrics, Kyoto University Graduate School of Medicine, 54 Kawahara-cho, Shogoin, Sakyo-ku, Kyoto, 606-8507 Japan; e-mail: yasumi@kuhp.kyoto-u.ac.jp or Hisanori Horiuchi, Department of Molecular and Cellular Biology, Institute of Development, Aging and Cancer, Tohoku University, 4-1 Seiryo-machi, Aoba-ku, Sendai 980-8575 Japan; e-mail: horiuchi@idac.tohoku.ac.jp.

References

1. Fischer A, Latour S, de Saint Basile G. Genetic defects affecting lymphocyte cytotoxicity. *Curr Opin Immunol.* 2007;19(3):348-353.
2. Hong W. Cytotoxic T lymphocyte exocytosis: bring on the SNAREs! *Trends Cell Biol.* 2005; 15(12):644-650.
3. Ménasché G, Feldmann J, Fischer A, de Saint Basile G. Primary hemophagocytic syndromes point to a direct link between lymphocyte cytotoxicity and homeostasis. *Immunol Rev.* 2005;203: 165-179.
4. Janka GE. Familial and acquired hemophagocytic lymphohistiocytosis. *Eur J Pediatr.* 2007; 166(2):95-109.
5. Gupta S, Weitzman S. Primary and secondary hemophagocytic lymphohistiocytosis: clinical features, pathogenesis and therapy. *Expert Rev Clin Immunol.* 2010;6(1):137-154.
6. Créput C, Galicier L, Buyse S, Azoulay E. Understanding organ dysfunction in hemophagocytic lymphohistiocytosis. *Intensive Care Med.* 2008; 34(7):1177-1187.
7. Stepp S, Dufourcq-Lagelouse R, Le Deist F, et al. Perforin gene defects in familial hemophagocytic lymphohistiocytosis. *Science.* 1999;286(5446): 1957-1959.
8. Feldmann J, Callebaut I, Raposo G, et al. Munc13-4 is essential for cytolytic granules fusion and is mutated in a form of familial hemophagocytic lymphohistiocytosis (FHL3). *Cell.* 2003; 115(4):461-473.
9. zur Stadt U, Schmidt S, Kasper B, et al. Linkage of familial hemophagocytic lymphohistiocytosis (FHL) type-4 to chromosome 6q24 and identification of mutations in syntaxin 11. *Hum Mol Genet.* 2005;14(6):827-834.
10. zur Stadt U, Rohr J, Seifert W, et al. Familial hemophagocytic lymphohistiocytosis type 5 (FHL-5) is caused by mutations in Munc18-2 and impaired binding to syntaxin 11. *Am J Hum Genet.* 2009; 85(4):482-492.
11. Côte M, Ménager M, Burgess A, et al. Munc18-2 deficiency causes familial hemophagocytic lymphohistiocytosis type 5 and impairs cytotoxic granule exocytosis in patient NK cells. *J Clin Invest.* 2009;119(12):3765-3773.
12. Cetica V, Pende D, Griffiths GM, Aricò M. Molecular basis of familial hemophagocytic lymphohistiocytosis. *Haematologica.* 2010;95(4):538-541.
13. Perez N, Virelizier JL, Arenzana-Seisdedos F, Fischer A, Griscelli C. Impaired natural killer activity in lymphohistiocytosis syndrome. *J Pediatr.* 1984;104(4):569-573.
14. Aricò M, Nespoli L, Maccario R, et al. Natural cytotoxicity impairment in familial haemophagocytic lymphohistiocytosis. *Arch Dis Child.* 1988;63(3): 292-296.
15. Schneider EM, Lorenz I, Müller-Rosenberger M, Steinbach G, Kron M, Janka-Schaub GE. Hemophagocytic lymphohistiocytosis is associated with deficiencies of cellular cytolysis but normal expression of transcripts relevant to killer-cell-induced apoptosis. *Blood.* 2002;100(8): 2891-2898.
16. Ishii E, Ueda I, Shirakawa R, et al. Genetic subtypes of familial hemophagocytic lymphohistiocytosis: correlations with clinical features and cytotoxic T lymphocyte/natural killer cell functions. *Blood.* 2005;105(9):3442-3448.
17. Schneider EM, Lorenz I, Walther P, Janka-Schaub GE. Natural killer deficiency: a minor or major factor in the manifestation of hemophagocytic lymphohistiocytosis? *J Pediatr Hematol Oncol.* 2003;25(9):680-683.
18. Grom AA, Villanueva J, Lee S, Goldmuntz EA, Passo MH, Filipovich A. Natural killer cell dysfunction in patients with systemic-onset juvenile rheumatoid arthritis and macrophage activation syndrome. *J Pediatr.* 2003;142(3):292-296.
19. Grom AA. Natural killer cell dysfunction: A common pathway in systemic-onset juvenile rheumatoid arthritis, macrophage activation syndrome, and hemophagocytic lymphohistiocytosis? *Arthritis Rheum.* 2004;50(3):689-698.
20. Horne A, Zheng C, Lorenz I, et al. Subtyping of natural killer cell cytotoxicity deficiencies in haemophagocytic lymphohistocytosis provides therapeutic guidance. *Br J Haematol.* 2005;129(5): 658-666.
21. Kogawa K, Lee SM, Villanueva J, Marmer D, Sumegi J, Filipovich AH. Perforin expression in cytotoxic lymphocytes from patients with hemophagocytic lymphohistiocytosis and their family members. *Blood.* 2002;99(1):61-66.
22. Alter G, Malenfant JM, Altfeld M. CD107a as a functional marker for the identification of natural killer cell activity. *J Immunol Methods.* 2004; 294(1-2):15-22.
23. Marcenaro S, Gallo F, Martini S, et al. Analysis of natural killer-cell function in familial hemophagocytic lymphohistiocytosis (FHL): defective CD107a surface expression heralds Munc13-4 defect and discriminates between genetic subtypes of the disease. *Blood.* 2006;108(7): 2316-2323.
24. Bryceson YT, Rudd E, Zheng C, et al. Defective cytotoxic lymphocyte degranulation in syntaxin-11 deficient familial hemophagocytic lymphohistiocytosis 4 (FHL4) patients. *Blood.* 2007;110(6): 1906-1915.
25. Shirakawa R, Higashi T, Tabuchi A, et al. Munc13-4 is a GTP-Rab27-binding protein regulating dense core granule secretion in platelets. *J Biol Chem.* 2004;279(11):10730-10737.
26. Febbraio M, Silverstein RL. Identification and characterization of LAMP-1 as an activation-dependent platelet surface glycoprotein. *J Biol Chem.* 1990;265(30):18531-18537.
27. Ren Q, Wimmer C, Chicka MC, et al. Munc13-4 is a limiting factor in the pathway required for platelet granule release and hemostasis. *Blood.* 2010; 116(6):869-877.
28. Nagai K, Yamamoto K, Fujiwara H, et al. Subtypes of familial hemophagocytic lymphohistiocytosis in Japan based on genetic and functional analyses of cytotoxic T lymphocytes. *PLoS ONE.* 2010;5(11):e14173.
29. Rohr J, Beutel K, Maul-Pavicic A, et al. Atypical familial hemophagocytic lymphohistiocytosis due to mutations in UNC13D and STXBP2 overlaps with primary immunodeficiency diseases. *Haematologica.* 2010;95(12):2080-2087.
30. Stinchcombe J, Bossi G, Griffiths G. Linking albinism and immunity: the secrets of secretory lysosomes. *Science.* 2004;305(5680):55-59.
31. Ren Q, Ye S, Whiteheart SW. The platelet release reaction: just when you thought platelet secretion was simple. *Curr Opin Hematol.* 2008;15(5): 537-541.

Anti-Aβ Drug Screening Platform Using Human iPS Cell-Derived Neurons for the Treatment of Alzheimer's Disease

Naoki Yahata[1,2], Masashi Asai[2,3,4], Shiho Kitaoka[1,2], Kazutoshi Takahashi[1], Isao Asaka[1,2], Hiroyuki Hioki[2,5], Takeshi Kaneko[5], Kei Maruyama[3], Takaomi C. Saido[4], Tatsutoshi Nakahata[1], Takashi Asada[6], Shinya Yamanaka[1,7], Nobuhisa Iwata[2,4,8]*, Haruhisa Inoue[1,2,7]*

1 Center for iPS Cell Research and Application, Kyoto University, Kyoto, Japan, **2** Core Research for Evolutional Science and Technology, Japan Science and Technology Agency, Saitama, Japan, **3** Department of Pharmacology, Faculty of Medicine, Saitama Medical University, Saitama, Japan, **4** Laboratory for Proteolytic Neuroscience, RIKEN Brain Science Institute, Saitama, Japan, **5** Department of Morphological Brain Science, Graduate School of Medicine, Kyoto University, Kyoto, Japan, **6** Department of Neuropsychiatry, Institute of Clinical Medicine, University of Tsukuba, Tsukuba, Japan, **7** Yamanaka iPS Cell Special Project, Japan Science and Technology Agency, Saitama, Japan, **8** Graduate School of Biomedical Sciences, Nagasaki University, Nagasaki, Japan

Abstract

Background: Alzheimer's disease (AD) is a neurodegenerative disorder that causes progressive memory and cognitive decline during middle to late adult life. The AD brain is characterized by deposition of amyloid β peptide (Aβ), which is produced from amyloid precursor protein by β- and γ-secretase (presenilin complex)-mediated sequential cleavage. Induced pluripotent stem (iPS) cells potentially provide an opportunity to generate a human cell-based model of AD that would be crucial for drug discovery as well as for investigating mechanisms of the disease.

Methodology/Principal Findings: We differentiated human iPS (hiPS) cells into neuronal cells expressing the forebrain marker, Foxg1, and the neocortical markers, Cux1, Satb2, Ctip2, and Tbr1. The iPS cell-derived neuronal cells also expressed amyloid precursor protein, β-secretase, and γ-secretase components, and were capable of secreting Aβ into the conditioned media. Aβ production was inhibited by β-secretase inhibitor, γ-secretase inhibitor (GSI), and an NSAID; however, there were different susceptibilities to all three drugs between early and late differentiation stages. At the early differentiation stage, GSI treatment caused a fast increase at lower dose (Aβ surge) and drastic decline of Aβ production.

Conclusions/Significance: These results indicate that the hiPS cell-derived neuronal cells express functional β- and γ-secretases involved in Aβ production; however, anti-Aβ drug screening using these hiPS cell-derived neuronal cells requires sufficient neuronal differentiation.

Citation: Yahata N, Asai M, Kitaoka S, Takahashi K, Asaka I, et al. (2011) Anti-Aβ Drug Screening Platform Using Human iPS Cell-Derived Neurons for the Treatment of Alzheimer's Disease. PLoS ONE 6(9): e25788. doi:10.1371/journal.pone.0025788

Editor: Hitoshi Okazawa, Tokyo Medical and Dental University, Japan

Received May 26, 2011; **Accepted** September 10, 2011; **Published** September 30, 2011

Funding: This study was supported by Core Research for Evolutional Science and Technology, Japan Science and Technology Agency (HI & NI), and a research grant from the NOVARTIS Foundation for Gerontological Research (HI). The funders had no role in study design, data collection and analysis, decision to publish, or preparation of the manuscript.

Competing Interests: The authors have declared that no competing interests exist.

* E-mail: haruhisa@cira.kyoto-u.ac.jp (HI); iwata-n@nagasaki-u.ac.jp (NI)

Introduction

Alzheimer's disease (AD) is the most common cause of dementia in the elderly. It is characterized clinically by progressive declines in memory, executive function, and cognition. It is also characterized by pathological features, including the deposition of amyloid plaques and neurofibrillary tangles as well as neuronal and synaptic loss in particular areas of the brain [1]. Accumulation of amyloid β peptide (Aβ) is hypothesized to initiate the pathogenic cascade that eventually leads to AD. The amyloid hypothesis is based on an imbalance between the production and clearance of Aβ [2]. Aβ is produced by β- and γ-secretase-mediated sequential proteolysis of amyloid precursor protein (APP) and plays a central role in AD pathogenesis. Because β- and γ-secretases are directly involved in Aβ production, they are straightforward and attractive therapeutic targets for AD. A number of compounds that inhibit or modulate these secretase activities and Aβ levels *in vitro* and *in vivo* have to date been developed [3,4].

Development of a human, cell-based *in vitro* assay system is a basic requisite for drug discovery and for investigating mechanisms of the disease. Induced pluripotent stem (iPS) cells reprogrammed from somatic cells [5,6] provide an opportunity to easily generate and use patient-specific differentiated cells. Because previous AD assay systems using human cancer cell lines or primary rodent cell cultures did not perfectly present the human intracellular environment or components, human iPS (hiPS) cell-derived neuronal cells may enable the development of more efficient drugs, such as γ-secretase modulators, and the better elucidation of AD mechanisms. In this study, we successfully generated forebrain neurons from hiPS cells, and showed that Aβ production in

neuronal cells was detectable and inhibited by some typical secretase inhibitors and modulators. Thus, we provide a new platform for AD drug development, which might be applied to AD patient-specific iPS cell research.

Results

Differentiation of forebrain neurons from hiPS cells

Recently, forebrain neurons were successfully differentiated from mouse embryonic stem (ES) cells [7,8,9] and human ES and/or iPS cells [9,10,11]. The methods used for differentiation into spinal motor neurons and midbrain dopaminergic neurons required the morphogens retinoic acid (RA)/sonic hedgehog (SHH) and fibroblast growth factor 8 (FGF8)/SHH, respectively [11,12]. On the other hand, non-morphogens [10,11] or Lefty A and Dickkopf homolog 1 (Dkk1) [7,9] have been used for the induction of hiPS cells into forebrain neurons. Because amyloid plaques are observed in the cerebral cortex from the early stage of AD development [13], stem cells should be differentiated to at least forebrain neurons for *in vitro* assays in AD research.

We differentiated forebrain neurons from hiPS 253G4 cells, which were generated from human dermal fibroblasts using three reprogramming factors (Oct3/4, Sox2, and Klf4) [14], as described previously (Figure 1A) [12,15]. When neural stem cells were induced with Noggin and SB431542 for 17 days, we obtained cells that were positive for the neuroectodermal marker, Nestin (Figure 1B), as previously reported using human and monkey ES cells [15]. After culturing the cells with morphogen-free medium for days 17–24, Forkhead box G1 (Foxg1) expression was induced and Foxg1-positive cells were observed (Figure 1C, D) [11,15]. We also examined whether treatment with cyclopamine, an SHH inhibitor, increased the number of neurons presenting a glutamatergic phenotype as observed in mouse ES cells [8]. The expression level of vesicular glutamate transporter 1 (vGlut1), a glutamatergic marker, was not significantly increased by the addition of cyclopamine (final concentration 1 μM) from days 17 to 24 (data not shown). Therefore, we did not add cyclopamine in this period in subsequent experiments. At day 24, dissociated cells were reseeded on 24-well plates to further characterize the cells.

Next, we evaluated the hiPS cell-derived neuronal cells using four cortical layer-specific markers, T-brain-1 (Tbr1) and chicken ovalbumin upstream promoter transcription factor (COUP-TF)-interacting protein 2 (Ctip2) [9,10,11], and cut-like homeobox 1 (Cux1) and special AT-rich sequence-binding protein 2 (Satb2) [16]. Quantitative polymerase chain reaction (qPCR) revealed that expression levels of these markers were increased in a differentiation day-dependent manner (Figure 1E). At day 52, all four of these markers were visualized by immunocytochemistry (ICC) (Figure 1F). The percentages of marker-positive cells relative to the total number of cells were 62.2±2.9% for Tbr1, 11.9±3.0% for Ctip2, 82.6±5.0% for Cux1, and46.0±7.1% for Satb2. The population of each marker-positive cell was similar to that of data reported previously in human fetal brain around gestational week-20 [16]. In this experimental schedule, most cells expressed one or a few neocortical markers at day 52.

Characterization of hiPS cell-derived neuronal cells

Cells that were reseeded at day 24, were sparsely adhered to the culture plate and had proliferated and extended neurites in a time course-dependent manner as observed by the neuronal marker, class-III β-tubulin (Tuj1), and microtubule-associated protein 2 (MAP2) (Figure 2A). Tuj1 expression was almost saturated at day 45 (Figure 2B), but MAP2 and synapsin I expression were still increasing (Figure 2C, D). Synaptic development continued until day 52, and many synapsin I-positive puncta were detected by ICC at day 52 (Figure 2A). Expression of the glial marker, glial fibrillary acidic protein (GFAP), was highest at day 52 in this schedule (Figure 2E). This sequential expression pattern is similar to that reported recently in human pluripotent stem cell-derived neurons; the synapsin I-positive neuronal and GFAP-positive glial cultures at day 52 corresponded to the stage at which spontaneous neuronal activity was observed [17].

We then examined the neurotransmitter phenotypes of these differentiated neurons by evaluating the synthesizing enzymes for two typical cortical neurotransmitters, glutamate and γ-aminobutyric acid (GABA). Expression of the glutamatergic neuronal marker, phosphate-activated glutaminase (PAG) [18], and the GABAergic neuronal marker, glutamate decarboxylase (GAD), were observed by ICC at day 52 (Figure 2F). PAG- and GAD-positive neurons comprised 60±20% and 5±4% of total cells, respectively. Most of the Tuj1-positive neurons were also co-localized with the punctate signals of vGlut1 (Figure 2G). GABA-positive neurons comprised a similar population to the GAD-positive ones (Figure 2F, H). On the other hand, cholineacetyltransferase (ChAT) or vesicular acetylcholine transporter (VAChT)-positive cholinergic neurons were little observed at day 52, although their mRNA level increased with differentiation time (Figure S1). These data showed that a majority of differentiated neuronal cells possessed a glutamatergic phenotype in the present condition.

Differentiated neuronal cells express some components related to Aβ production

To evaluate their usefulness as an AD model, we measured the levels of Aβ secreted from the differentiated neuronal cells at days 38, 45, and 52. In the non-amyloidogenic pathway, α-secretase cleaves full-length APP (FL-APP) within the Aβ domain to the large soluble APP fragment (sAPPα) and APP-C terminal fragment α (CTFα) (Figure 3) [19]. In the amyloidogenic pathway, β-secretase, β-site APP cleaving enzyme 1 (BACE1), cleaves APP on the N-terminal side of the Aβ domain to soluble sAPPβ and APP-CTFβ (Figure 3). FL-APP and its cleavage products were increased in a time-course-dependent manner (Figure 3).

APP has three alternatively spliced isoforms: APP695, APP751, and APP770. APP695 is most abundantly expressed in neurons, whereas APP751 and APP770 show more ubiquitous expression patterns [20]. In cell lysates, we detected three separate APP variants on western blots. The estimated percentages of the neuron-dominant variant APP695 were 64.5±1.0%, 68.6±2.2%, and 69.6±2.1% at days 38, 45, and 52, respectively (Figures 3A and S2). The neuronal population at day 52 was approximately consistent with the sum of the percentages of the glutamatergic and GABAergic neurons mentioned above.

The aspartyl protease BACE1, the major β-secretase involved in cleaving APP, is a significant molecule for AD pathology because BACE1 protein levels and activity are increased in the brains of patients with the sporadic form of AD [21]. In our differentiated neurons, BACE1 protein levels were increased in a time course-dependent manner (Figure 4A, B), and we speculated that the upregulation of BACE1 protein levels may be due to a posttranscriptional mechanism [22]. BACE1 mRNA levels were slightly elevated with time (Figure 4B). These data may indicate that increased BACE1 protein levels were mainly induced by translational activation along with neuronal differentiation.

APP-CTFβ is cleaved to Aβ and APP intercellular domain (AICD) by γ-secretase (Figure 3). The γ-secretase complex consists of four core members, presenilin (PS; either PS1 or PS2), nicastrin, Pen-2, and Aph-1 [23]. PS1, nicastrin, and Pen-2 were detected by

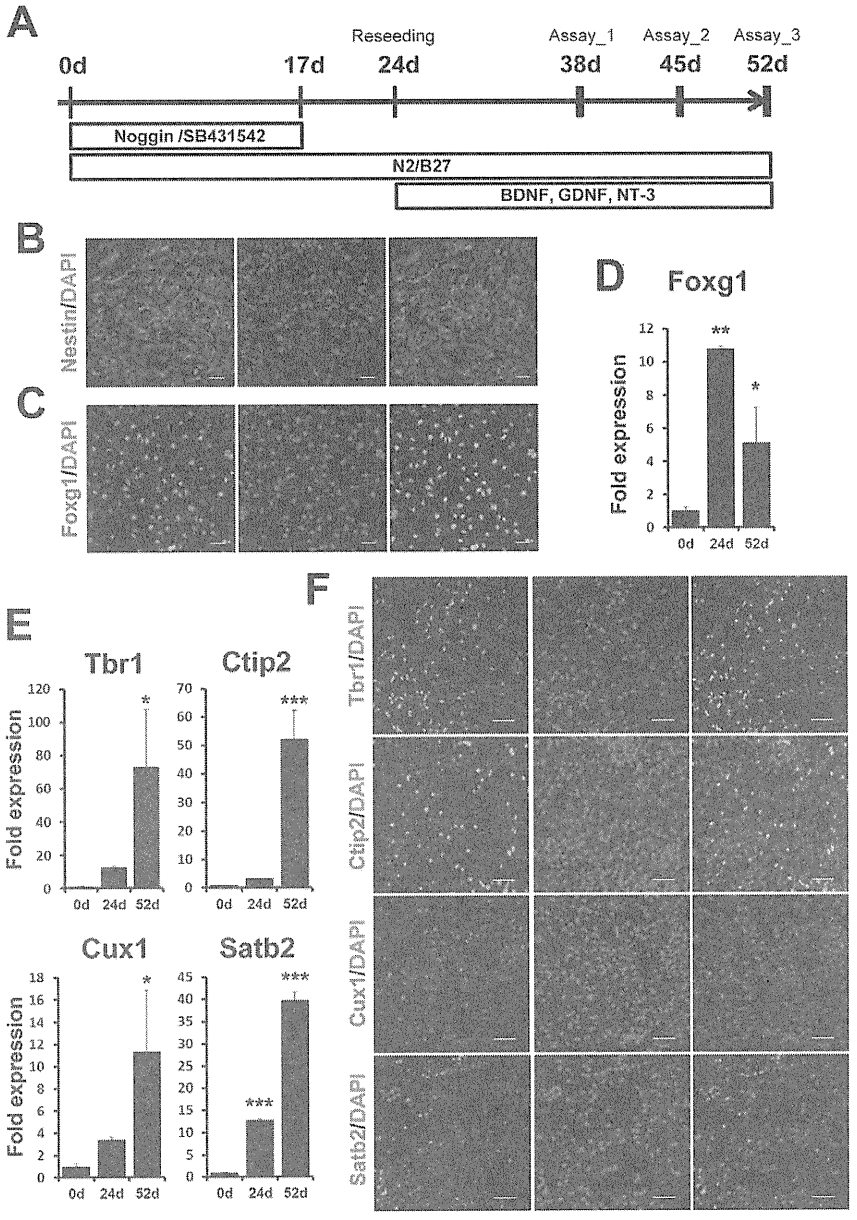

Figure 1. Differentiation of forebrain neurons from hiPS cells. (A) Experimental scheme of neural differentiation from hiPS cells, 253G4. Nestin-positive neuroepithelial cells (B) and Foxg1-positive cells (C) were observed at days 17 and 24, respectively. Scale bar, 50 μm. Expression levels of Foxg1 (D) and the neocortical markers Tbr1, Ctip2, Cux1, and Satb2 (E) at days 0, 24, and 52. Expression levels were measured by qPCR and normalized by that of GAPDH. "Fold expression" is shown as a ratio of day 24/day 0 or day52/day 0. Each column represents the mean ± SD of 3 assays. $^{*}p<0.05$, $^{**}p<0.01$, $^{***}p<0.001$, significantly different from day 0 by Dunnett's test. (F) ICC staining of Tbr1-, Ctip2-, Cux1- and Satb2-positive cells at day 52. Scale bar, 50 μm.
doi:10.1371/journal.pone.0025788.g001

western blotting, but their expression levels did not change markedly over time (Figure 4A, C). Aph-1 has two isoforms in human, Aph-1A and Aph-1B, which are considered to have different effects on the production of Aβ species related to AD [24]. Their expression levels measured by qPCR were relatively constant (Figure 4D). The Aph-1B/Aph-1A ratios also did not show significant differences among the time points analyzed here (Figure 4E).

Aβ has several species, including Aβ40 and Aβ42, which have emerged as two of the most robust Aβ measurements in brain. Recent studies suggest that Aβ40 and Aβ42 may have different effects on Aβ aggregation or oligomerization [25,26]. We measured Aβ40 and Aβ42 secreted into conditioned media for 2 days by sandwich ELISA. Both types of Aβ increased with time (Figure 5A). The level of Aβ40 was higher than that of Aβ42, compatible with previous reports [4,27,28,29,30]. Interestingly, the ratio of Aβ42/Aβ40 was highest at day 38, and there was no significant difference between days 45 and 52 (Figure 5B).

Inhibition of Aβ40 and Aβ42 secretion

We examined whether the differentiated neurons contained funtional β- and γ-secretases and whether Aβ secretion could be controlled. We selected the most effective, commercially available β- and γ-secretase inhibitors, β-secretase inhibitor IV (BSI) [31]

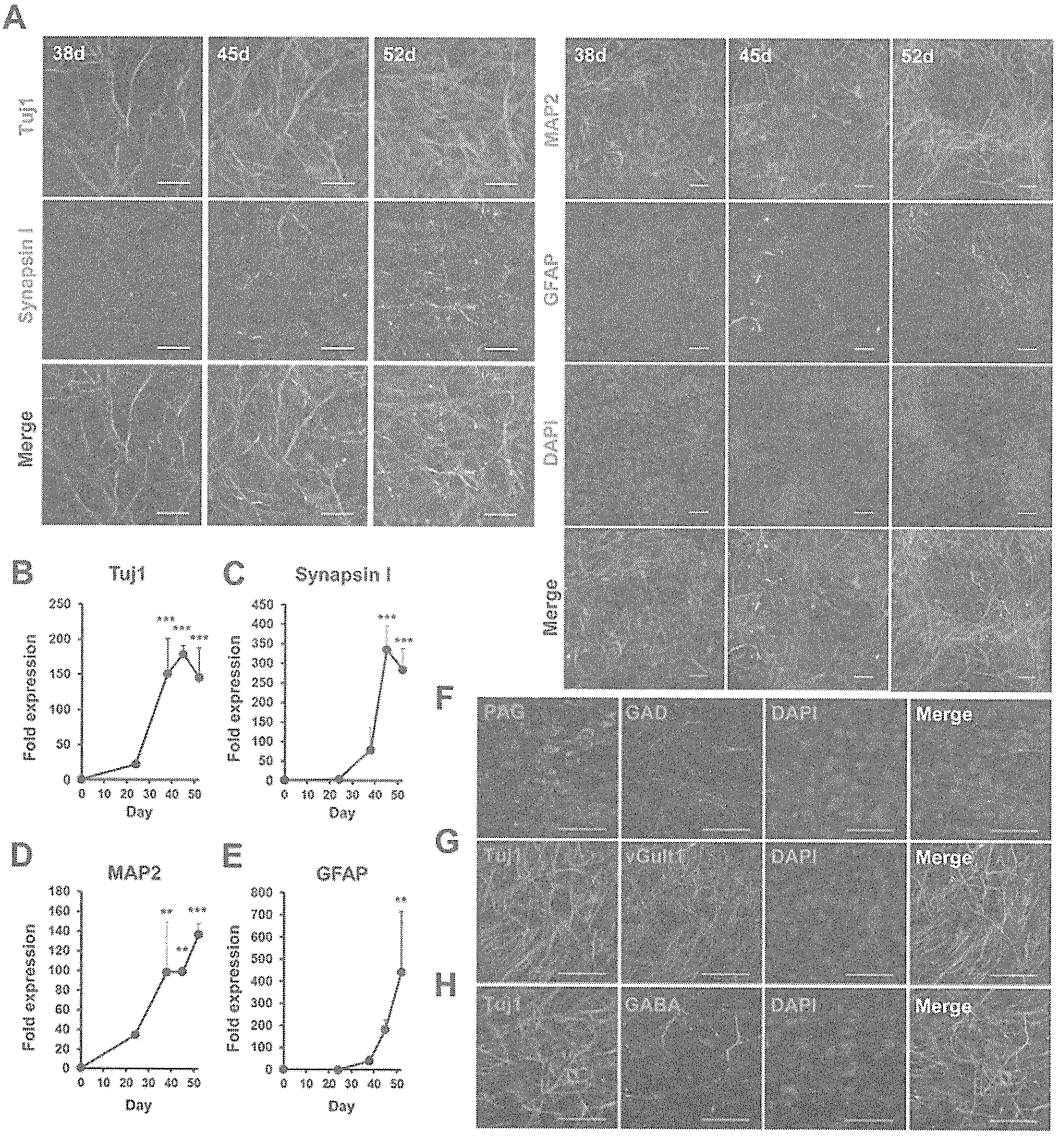

Figure 2. Characterization of neuronal and glial cells differentiated from hiPS cells. (A) Time-dependent morphological changes of cells reseeded in a 24-well plate. Neuronal and glial cells were stained by anti-Tuj1 (left; red), anti-synapsin I (left; green), anti-MAP2 (right; red), and anti-GFAP (right; green) antibodies and DAPI (right; blue) at 38, 45, and 52 days. Scale bar, left; 20 μm, right; 50 μm. Expression levels of Tuj1 (B), synapsin I (C), MAP2 (D), and GFAP (E) at days 0, 24, 38, 45, and 52 were measured by qPCR and normalized by that of GAPDH. "Fold expression" is the ratio of expression at each day compared to day 0. Each point represents mean ± SD of 3 assays. $^{*}p<0.05$, $^{**}p<0.01$, $^{***}p<0.001$, significantly different from day 0 by Dunnett's test. (F–H) Neurotransmitter phenotypes at day 52. PAG (red)- and GAD (green)-positive (F), vGlut1 (green)- and Tuj1 (red)-positive (G), and GABA (green)- and Tuj1 (red)-positive cells (H). Blue, DAPI. Scale bar, 50 μm.
doi:10.1371/journal.pone.0025788.g002

and γ-secretase inhibitor XXI/Compound E (GSI) [32], respectively. We also examined the effect of a non-steroidal anti-inflammatory drug (NSAID), sulindac sulfide [33], because some NSAIDs directly modulate γ-secretase activity to selectively lower Aβ42 levels [33,34]. The cells were treated with each drug for 2 days, and Aβ was monitored in the collected media at day 38 or 52.

There were different susceptibilities to all three drugs between days 38 and 52 (Figure 6) as revealed by two-way analysis of variance (ANOVA) [significant interaction between day and dose (BSI, $p<0.001$ in Aβ40 and Aβ42, respectively; GSI, $p<0.001$ in Aβ40 and Aβ42, respectively; NSAID, $p<0.001$ in Aβ42)]. Following BSI and NSAID treatment, secretion of Aβ40 and Aβ42 was decreased in a dose-dependent manner (Figure 6A, B, E, and F). NSAID especially showed more efficient inhibition of Aβ42 than that of Aβ40, consistent with a previous report [33]. Following GSI treatment (Figure 6C, D), secretion of both Aβ40 and Aβ42 was increased at lower doses (10^{-11}–10^{-8} M), but was inhibited at higher doses (10^{-7}–10^{-6} M) at day 52. This phenomenon, which is called a "gradual Aβ rise", was observed following the addition of other GSIs in a cell line system [35]. On the other hand, secretion of both Aβ40 and Aβ42 at day 38 showed a fast increase at lower doses (10^{-11}–10^{-9} M) (Aβ surge) and drastic decline at 10^{-8} M. We also examined the effects of these inhibitors on cell viability using the lactate dehydrogenase (LDH) assay. Two-day-treatments with the highest concentrations

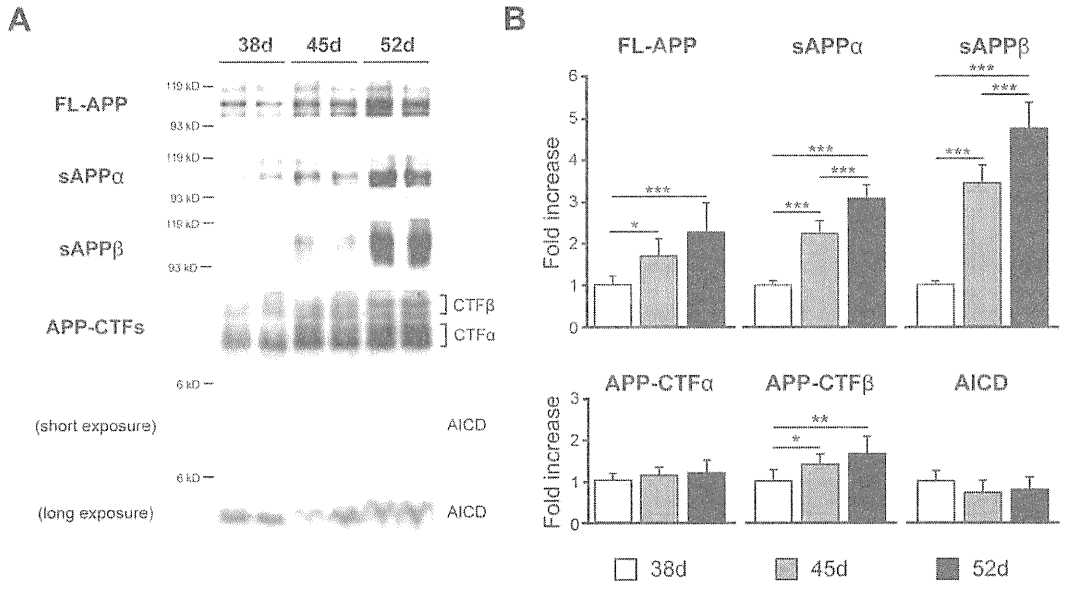

Figure 3. APP was expressed in hiPS cell-derived neuronal cells. HiPS cell-derived neuronal cells express full-length APP, sAPPα, sAPPβ, APP-CTFα, APP-CTFβ and AICD at 38, 45, and 52 days. (A) Representative western blots of APP and its fragments. (B) Each column represents mean ± SD of 8 samples measured by quantitative western blot analysis and normalized by that of β-actin. "Fold expression" represents the ratio of expression on the given day compared to day 38. $^{*}p<0.05$, $^{**}p<0.01$, $^{***}p<0.001$, Tukey's test.
doi:10.1371/journal.pone.0025788.g003

of BSI, GSI, or NSAID did not induce cell death (Table S1). We also traced these experiments using human ES (hES) cell (H9)-derived neuronal cells (Figure S4) because remaining expression of reprogramming factors, Oct3/4 and Klf4, were observed in hiPS cell (253G4)-derived neuronal cells (Figure S6). The Aβ production and its inhibition by these drugs in hES cell-derived neuronal cells were relatively similar to those in hiPS cell-derived ones (Figure S5). These data showed that BSI, GSI, and NSAID partially or fully blocked Aβ production in the hiPS cell-derived neuronal cells, indicating that these cells expressed functional β- and γ-secretases.

Discussion

AD is the most common cause of dementia in the elderly, with progressive neuronal loss in the cerebral cortex and hippocampal formation. Although the underlying etiology of most AD remains unclear, Aβ is thought to play a pivotal role in its pathogenesis. Studies from animal and cellular models have shown that mutations in the APP, PS1, and PS2 genes affected the production of Aβ, which contributes to the formation of amyloid plaques [19]. In several strains of mouse models, Aβ levels in brain tissue, cerebrospinal fluid (CSF), and plasma have been associated with AD pathogenesis and cognitive impairment [27,28,36]. Human samples from clinical AD patients have also been used for pathological and biochemical analyses to understand the etiology of AD. Aβ levels in CSF and plasma have been examined to evaluate their risks for AD [29,37], but brain tissues are only available postmortem for such analyses. On the other hand, immortalized human cell lines derived from kidney or brain, primary neurons derived from mice and rats, or cells artificially overexpressing APP or presenilin with or without familial AD mutations have been utilized for *in vitro* studies [4,30]. There is no doubt that these cells are quite different from living neurons in the human body in terms of innate qualities. Although we have had no choice until recently, important advances in technology of iPS cells may now provide the opportunity to use intact human-derived neuronal cells [38].

We evaluated whether iPS cell-derived neuronal cells could be applied to an *in vitro* cell-based assay system for AD research. In particular, further investigations into the metabolic mechanisms of Aβ are requisite for drug development to treat the brains of patients afflicted with AD. In this respect, we provide a profile of the molecular components associated with Aβ production in hiPS cell-derived neuronal cells and propose to add an Aβ assay system using these cells to the panel of generalized Aβ-monitoring systems (Table 1). Human neuronal cells are considered to provide more accurate human neuronal conditions within which to evaluate drug efficacy or toxicity than other human cell lines (e.g., cancer lines). Furthermore, we would be able to investigate how hiPS cell-derived neuronal cells reflect AD-related physiological and pathological conditions based on Aβ production.

In the present study, we characterized iPS cell-derived neuronal cells in terms of their expression of neuronal and glial markers by exposing them to Noggin and SB431542 during their differentiation (Figures 1 and 2). We observed increases in GFAP mRNA levels and in synapsin I-positive synaptic puncta at day 52. This was consistent with data showing that the existence of astrocytes promotes synaptic activity in human ES cell-derived neurons [40]. When differentiation occurred in the presence of non-morphogens, we obtained mainly glutamatergic neurons (Figure 2F, G), quite in line with previous reports of concerning hES and hiPS cells [10,11]. Expression of the forebrain marker Foxg1 suggests a default forebrain identity of the 253G4 iPS cells used in this study (Figure 1C, D). We also observed the expression of the neocortex-specific transcriptional factors Tbr1, Ctip2, Cux1, and Satb2 (Figure 1E, F). These expression schemes appear to mimic human neocortical development *in vitro* [16], although further analyses are needed to assist in understanding human neuronal subtype-specific differentiation.

This is the first study to observe the expression of APP, β- and γ-secretase, and the production of Aβ in hiPS cell-derived neuronal

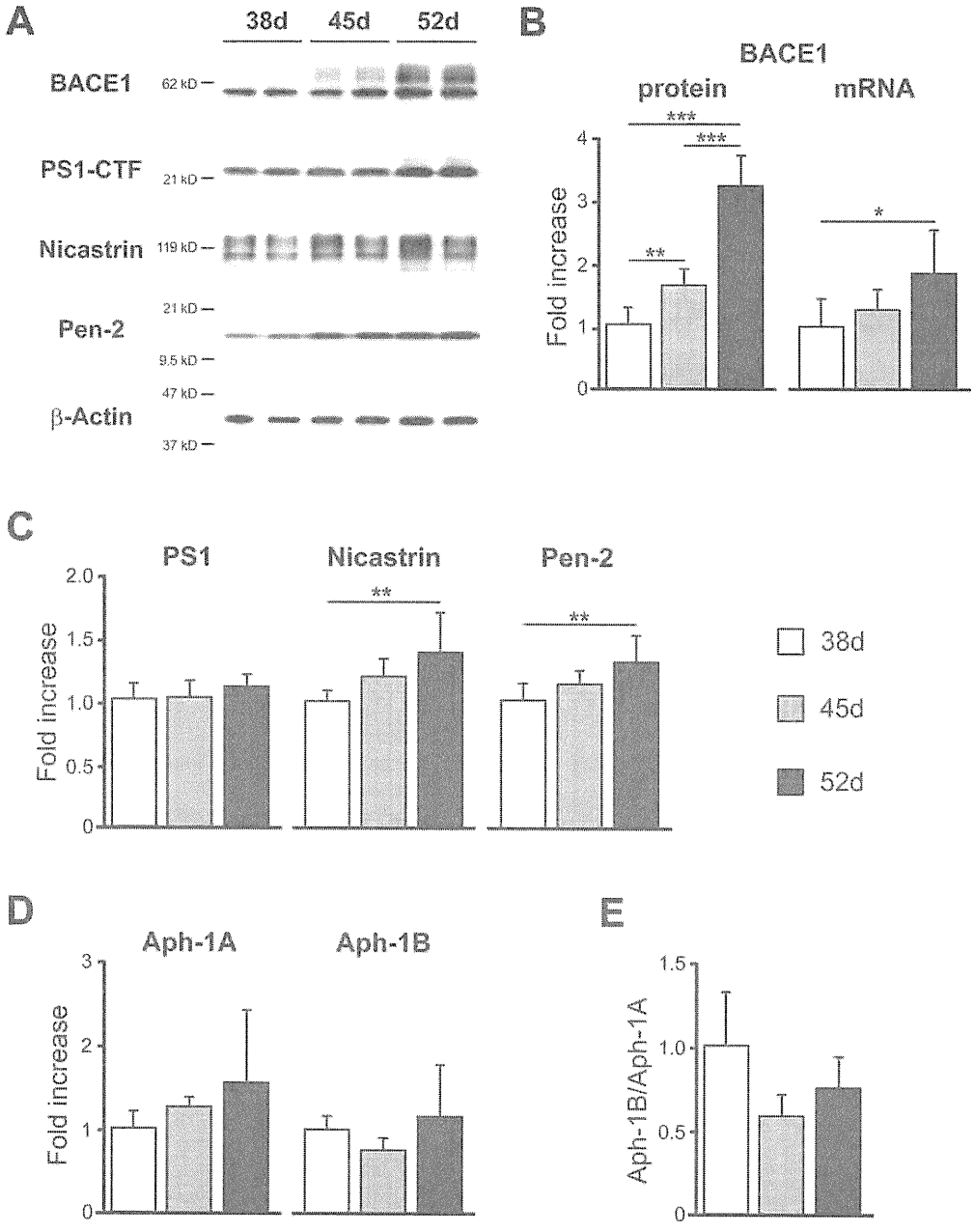

Figure 4. β-Secretase and γ-secretase components were expressed in hiPS cell-derived neuronal cells. The hiPS cell-derived neuronal cells express BACE1 protein and mRNA (B), γ-secretase components; presenilin 1(PS1), nicastrin, Pen-2 (C), and Aph-1A, and Aph-1B (D) at days 38, 45, and 52. Expression levels were quantified by western blot analysis (n = 8) (B, C) or qPCR (n = 3) (D) and normalized by that of β-actin. "Fold expression" represents the ratio of expression on the given day compared to day 38. (E) The ratio Aph-1B/Aph-1A. Data represent mean ± SD. (A) Representative western blots of BACE1 and γ-secretase components at 38, 45, and 52 days. $^{*}p<0.05$, $^{**}p<0.01$, $^{***}p<0.001$, Tukey's test.
doi:10.1371/journal.pone.0025788.g004

cells. APP, sAPPβ, APP-CTFβ and BACE1 protein levels were increased (Figures 3 and 4), but protein levels of γ-secretase components were not significantly different during the period from day 38 to 52 (Figure 4C, D). Aβ production in hiPS cell 253G4-derived neuronal cells increased with differentiation course (Figure 5A), however that in another hiPS cell 201B7 [5]- and in hES H9-derived neuronal cells did not increase (Figures S5 and S7) although all cell lines showed development of synapse (Figure S4A) as Aβ releasing site [41], indicating that besides synaptogenesis, subtle changes in localization and assembly of APP [42], BACE1, γ-secretase components would be critical for Aβ production.

The Aβ42/Aβ40 ratio unexpectedly showed a significant decrease from day 38 to 45 (Figure 5B). Serneels *et al.* reported that the γ-secretase complex containing Aph-1B was active and involved in the generation of amyloidogenic Aβ42 [24]. Our data showed that the Aph-1B/Aph-1A ratio did not change significantly with cell differentiation (Figure 4E); therefore, the Aβ42/Aβ40 ratio may be influenced by other unknown factors interacting directly or indirectly with γ-secretase.

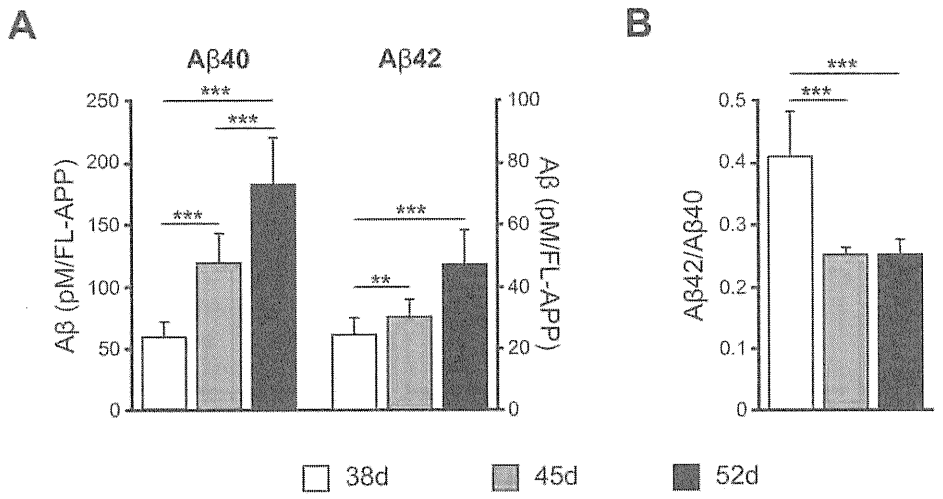

Figure 5. Aβ was produced in hiPS cell-derived neuronal cells. (A) Aβ40 or Aβ42 secreted into the conditioned media and FL-APP were measured by sandwich ELISA and western blot analysis, respectively. Expression level of Aβ was normalized by that of FL-APP. (B) Aβ42/Aβ40 ratios. Data represent the mean ± SD of 8 assays. *, $^{\#}p<0.05$, **, $^{\#\#}p<0.01$, ***, $^{\#\#\#}p<0.001$, Tukey's test.
doi:10.1371/journal.pone.0025788.g005

BSI, GSI, and the NSAID sulindac sulfide inhibited Aβ production in this human neuronal cell system (Figure 6). The inhibitory effect on Aβ production by GSI showed a characteristic difference between days 38 (Aβ surge) and 52 (gradual Aβ rise) (Figure 6C, D). Aβ surge at day 38 was also observed in another hiPS cell (201B7)-derived neuronal cells (Figure S7) as well as in hES cell line, H9-derived ones (Figure S5). At day 38, GSI might promote neuronal differentiation with synaptogenesis via blocking Notch signaling [43] rather than inhibition of Aβ production, leading to Aβ surge. Another possible explanation for Aβ surge is that change in conformation or components of the γ-secretase affects the sensitivity of γ-secretase to GSI (total Aβ, Aβ40, Aβ42, and Aβ42/Aβ40), although levels of mRNA and the ration for Aph-1A and Aph-1B do not change between days 38 and 52 (Figure 4D, E) Thus, for precise Aβ monitoring in human stem cell-derived neuronal cells, it is necessary to use neuronal cells with a sufficient substrate level and synaptogenesis, because Aβ is released presynaptically, as mentioned above.

Some NSAIDs are known to preferentially lower Aβ42 [33,34]. Our data showed that sulindac sulfide was capable of inhibiting Aβ42 secretion at high concentrations ($\geq 10^{-5}$ M) (Figure 6F), although a few NSAIDs do not show therapeutic effects for AD. Negative results might be due to low γ-secretase modulator potency [44]. To discover novel effective drugs for modulating β- or γ-secretase activity, the *in vitro* hiPS cell-derived neuronal cell assay system might be expected to yield such drugs.

Familial AD patient specific neuronal cells generated by direct conversion (induced neuron, iN) show higher Aβ42/Aβ40 ratio than those of unaffected individuals [45]. Based on this report, hiPS/hES cell-derived neurons expressing mutant PS1, PS2, or APP may show higher Aβ42/Aβ40 ratio. Comparing to our results, the levels of Aβs in this assay (Aβ40; ~1.7 ng/ml at day 52) is higher than that using iN cells (Aβ40; ~0.1 ng/ml), although iN cells become functional neurons more quickly. The optimization of neuronal cell condition for comparison of the Aβ42/Aβ40 ratio between multiple iPS cell-derived neuronal cells may be required.

In conclusion, our findings indicate that hiPS cell-derived neuronal cells express functional β- and γ-secretases related to the production of Aβ in the present experimental conditions. In addition, our data provide the proof in principle that hiPS cell-derived neuronal cells can be applied to drug screening and AD patient-specific iPS cell research.

Materials and Methods

Antibodies and reagents

Primary antibodies used were as follows: mouse anti-Nestin (1:200, Millipore, Temecula, CA), mouse anti-Tuj1 (1:2000, Covance, Princeton, NJ), rabbit anti-GFAP (1:500, DAKO, Carpinteria, CA), rabbit anti-Synapsin I (1:500, Millipore), mouse anti-Cux1 (1:100, Abnova, Taipei, Taiwan), rabbit anti-Satb2 (1:1000, Abcam, Cambridge, UK), rat anti-Ctip2 (1:500, Abcam), rabbit anti-Tbr1 (1:500, Abcam), rabbit anti-vGlut1 (1:1000, Synaptic Systems, Göttingen, Germany), rabbit anti-Foxg1 (1:100, Abcam), rabbit anti-GABA (1:1000, Sigma-Aldrich, St. Louis, MO), rabbit anti-GAD65/67 (1:200, Millipore), mouse anti-PAG [46] (1:500), rabbit anti-APP (1:15000, Sigma-Aldrich), mouse anti-APP (1 μg/ml, Millipore), rabbit-anti BACE (1:2000, Merck, Darmstadt, Germany) mouse anti-PS1 loop C-terminus (1:1000, Millipore), rabbit anti-nicastrin (1 μg/ml, Thermo Scientific, Rockford, IL), rabbit anti-Pen-2 (1:1000, Invitrogen, San Diego, CA), mouse anti-MAP2 (1:200, Millipore), goat anti-ChAT (1:100, Millipore), guinea pig anti-VAChT (1:500, Millipore), and mouse anti-β-actin (1:15000, Sigma-Aldrich). We raised rabbit polyclonal antibodies against the carboxyl terminals of human sAPPα (hsAPPα) and sAPPβ using the KLH-conjugated synthetic peptides CRHDSGYEVHHQK and CKTEEISEVKM, respectively (Figure S3). All animal experiments were performed in compliance with the institutional guidelines at RIKEN Brain Science Institute, and were approved by the Animal Care and Use Committee (Permit number: H17-2B031). Each antibody was purified with a peptide-conjugated column [47]. Alexa Fluor 488 and Alexa Fluor 594-conjugated secondary antibodies (Invitrogen) were used for immunofluorescence.

The β-secretase inhibitor IV [31] and γ-secretase inhibitor XXI/Compound E [32] were purchased from Merck. Sulindac sulfide (NSAID) was purchased from Sigma-Aldrich.

Immunocytochemistry

Cells were fixed with 4% paraformaldehyde in phosphate buffered saline (PBS) for 30 min, and incubated in PBS

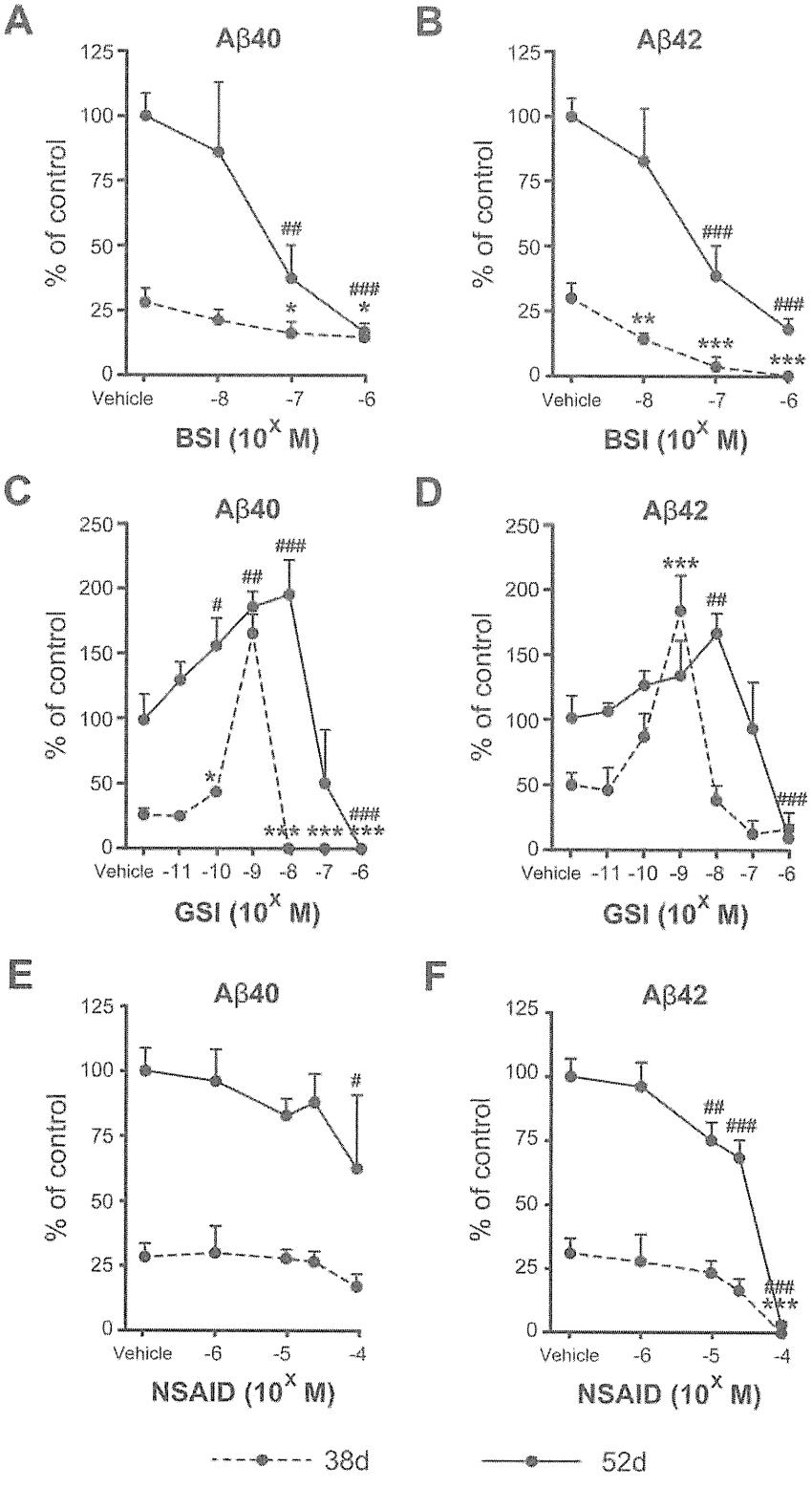

Figure 6. Aβ production was modulated by β- and γ-secretase inhibitors and an NSAID. β-Secretase inhibitor (BSI) (A, B), γ-secretase inhibitor (GSI) (C, D), and NSAID (E, F) were added into hiPS cell-derived neuronal cell cultures at day 36 (dotted line) and 50 (bold line), and two days later amounts of Aβ40 and Aβ42 secreted into the conditioned media were measured. The ratios Aβ40/FL-APP and Aβ42/FL-APP are expressed as percentages of the vehicle-treated group at day 52 and represent mean ± SD of 3 assays. A, B: There were significant main effects of day ($F(1, 16) = 72.5$ and 162.4, $p<0.001$ in Aβ40 and Aβ42, respectively) and dose ($F(3, 16) = 23.1$ and 45.7, $p<0.001$ in Aβ40 and Aβ42, respectively), and significant interaction between day and dose ($F(3, 16) = 13.0$ and 11.7, $p<0.001$ in Aβ40 and Aβ42, respectively) by 2-way ANOVA. C, D: There were significant main effects of day ($F(1, 28) = 240.5$ and 59.1, $p<0.001$ in Aβ40 and Aβ42, respectively) and dose ($F(6, 28) = 70.8$ and 37.8, $p<0.001$ in Aβ40 and Aβ42, respectively), and significant interaction between day and dose ($F(6, 28) = 23.5$ and 15.1, $p<0.001$ in Aβ40 and Aβ42, respectively) by

2-way ANOVA. E, F: There were significant main effects of day ($F(1, 20) = 196.9$ and 418.0, $p<0.001$ in Aβ40 and Aβ42, respectively) and dose ($F(4, 20) = 4.16$, $p = 0.013$ and $F(4, 20) = 91.9$, $p<0.001$ in Aβ40 and Aβ42, respectively), and significant interaction between day and dose ($F(4, 20) = 25.4$, $p<0.001$ in Aβ42) by 2-way ANOVA. *, $^{\#}p<0.05$, **, $^{\#\#}p<0.01$, ***, $^{\#\#\#}p<0.001$, significantly different from respective vehicle-treated groups by Dunnett's test.
doi:10.1371/journal.pone.0025788.g006

containing 0.2% Triton X-100 for 10 min (permeabilization). After blocking with 2% BSA in PBS, cells were incubated with primary antibody diluted with blocking buffer and then washed with PBS. Finally the cells were incubated with secondary antibodies and mounted using ProLong Gold antifade reagent with DAPI (Invitrogen). The immunoreactive cells were visualized using an LSM 700 Laser Scanning Microscope (Carl Zeiss, Jena, Germany) and a Biorevo BZ-9000 fluorescence microscope (Keyence, Osaka, Japan).

Quantitative real-time RT-PCR

Total RNA was isolated from cells using TRIZOL reagent (Invitrogen). Contaminating DNA was removed using the TURBO DNA-free kit (Ambion, Austin, TX), and cDNA was synthesized using ReverTra Ace-α (Toyobo, Osaka, Japan), according to the manufacturers' protocols. Real-time PCR was performed using the StepOnePlus system (Applied Biosystems) and SYBR green reagent (TAKARA, Shiga, Japan). The primers used are listed in Table S2 in the supporting information.

HiPS cell culture and differentiation into neuronal cells

HiPS cells, 253G4 [14] (passage 20–30) or hES cells, H9 were cultured on mitomycin C-treated mouse embryonic fibroblasts in primate ES medium (ReproCELL, Kanagawa, Japan) supplemented with bFGF (Wako Pure Chemicals, Osaka, Japan). To obtain cortical neurons derived from iPS cells, we partially modified a previous method [12,15]. For neural induction, partially dissociated iPS cell colonies, 40–100 μm in diameter, were selected with Cell Strainer (BD Falcon, BD Bioscience, Bedford, MA) and plated on poly-L-lysine (Sigma-Aldrich)/Laminin (BD Biosciences) (PLL/LM)-coated dishes (P1) in N2B27 neuronal differentiation medium [DMEM/F12 (Invitrogen), Neurobasal (Invitrogen), N2 (Invitrogen), B27 minus vitamin A (Invitrogen), L-Gln (Invitrogen)], supplemented with 100 ng/ml human recombinant Noggin (R&D Systems, Minneapolis, MN) and 1 μM SB431542 (Sigma-Aldrich) for 17 days. At day 10, primary colonies were split into small clumps using 200 U/ml collagenase with $CaCl_2$ and plated into PLL/Entactin-Collagen IV-Laminin (Millipore) (ECL)-coated dishes (P2). At day 17, P2 cells were dissociated using Accutase (Innovative Cell Technologies, San Diego, CA) and cultured on PLL/ECL-coated dishes (P3). Finally, at day 24, cells dissociated with Accutase were passed through a 40-μm cell strainer (BD Biosciences), counted, and cultured on PLL/LM/Fibronectin (Millipore)-coated 24-well plates at 2.5×10^4 cells/well in N2B27 medium supplemented with 10 ng/ml BDNF, GDNF, and NT-3 (R&D Systems). Medium changes for cell culture were carried out once every two or three days until day 52.

Aβ sandwich ELISA

At days 38, 45, and 52, two-day incubated conditioned media were collected from cultured neuronal cells and centrifuged at 4,000 *g* for 10 min. The resultant clear supernatants were subjected to sandwich ELISA (Wako) with a combination of monoclonal antibodies specific to the midportion of Aβ and specific to the C-terminal of Aβ40 or Aβ42, to determine the amounts of secreted Aβ, as described previously [20,28,30]. We also examined the inhibitory effect of each drug on Aβ production. All media were replaced with new media containing each drug and two-day conditioned media were analyzed as mentioned above.

Western blot analysis

Western blot analysis was performed as previously described with minor modification. In addition to conditioned media, cell lysates were also collected, extensively washed with PBS, and lysed

Table 1. Panel of Aβ monitoring systems.

Human sample	**Aβ40**	**Aβ42**	**Ref.**
Brain tissue [AD]	↑ (AD/NC)	↑ (AD/NC)	[39]
CSF [AD]	-	↓ (AD/NC)	[37]
	→ (AD/NC)	↓ (AD/NC)	[29]
Plasma [AD]	↑ (AD/NC)	→ (AD/NC)	[29]
iPS cell-derived neuronal cells	Measurable	Measurable	This report
Mouse model	**Aβ40**	**Aβ42**	**Ref.**
Brain [PDAPP]	↑ (Aging)	↑ (Aging)	[36]
Brain [APP23]	↑ (Tg/non-Tg)	↑ (Tg/non-Tg)	[27]
Brain [Tg2576]	↑ (Aging)	↑ (Aging)	[28]
	↑ (Tg/non-Tg)	↑ (Tg/non-Tg)	
CSF [Tg2576]	↓ (Aging)	↓ (Aging)	[28]
Plasma [Tg2576]	↓ (Aging)	↓ (Aging)	[28]
Cell line	**Aβ40**	**Aβ42**	**Ref.**
[APP_{NL}-H4]	Measurable	Measurable	[30]
[CHO-APP_{NL}/SH-SY5Y-APP]	Measurable	Measurable	[4]

AD, Alzheimer's disease; NC, normal control; Tg, transgenic mouse model.
doi:10.1371/journal.pone.0025788.t001

directly with 1× sample buffer (EzApply; ATTO, Tokyo, Japan). The media or cell lysates were separated by 5–20% gradient or 7.5% [FL-APP] or 10% [β-actin] sodium dodecyl sulfate-polyacrylamide gel electrophoresis (SDS-PAGE) and transferred to polyvinylidene difluoride membranes (Hybond-P; GE Healthcare, Buckinghamshire, UK). The blots were probed with an appropriate primary antibody, followed by HRP-conjugated anti-mouse or anti-rabbit IgG (GE Healthcare). The protein bands were visualized using an enhanced chemiluminescence (ECL) detection method (GE Healthcare), and band intensity was analyzed with a densitometer (LAS-4000; GE Healthcare), using the Science Laboratory 2001 Image Gauge software (Fujifilm, Tokyo, Japan). Immunoreactive protein content in each sample was calculated based on a standard curve constructed with each recombinant protein or one of the samples. Each set of experiments was repeated at least two times to confirm the results. The level of β-actin protein, measured by quantitative western blotting using β-actin antibody, was used as an extraction and loading control.

LDH assay

Cell toxicity assays were performed using a cytotoxicity detection kit (LDH, Roche, Mannheim, Germany) according to the manufacturer's protocol.

Statistical analysis

All data were expressed as mean ± SD. Comparisons of mean among more than three groups were done by one-way or two-way ANOVA, followed by *post-hoc* test (PRISM, GraphPad software). *P* values ≤0.05 indicated significant differences.

Supporting Information

Figure S1 Cholinergic neuronal marker-positive cells were observed in hiPS cell-derived neuronal cells. Expression levels of ChAT (A) and VAChT (B) were quantified by qPCR (n = 3) and normalized by that of GAPDH. "Fold expression" represents the ratio of expression on the given day compared to day 38. ChAT- (C) and VAChT (D)-positive cells were observed a little at day 52.
(TIF)

Figure S2 Percentages of the three isoforms of APP (APP770, APP751, and APP695) at 38, 45, and 52 days. Each column represents mean ± SD of 8 assays. $^{*}p<0.05$, $^{**}p<0.01$, $^{***}p<0.001$, Tukey's test.
(TIF)

Figure S3 New hsAPPα and sAPPβ antibodies specifically detect human sAPPα and sAPPβ by western blots, respectively. Human neuroglioma H4 cells overexpressing wild-type APP (APP_{WT}-H4 cells) were treated with α-secretase activator (12-*O*-tetradecanoylphorbol 13-acetate (TPA)), α-secretase inhibitor (TNF-α protease inhibitor-2 (TAPI-2)), or β-secretase inhibitor (see Protocol S1). Brain lysates of APP-knockout mice (APP-KO) were used as negative control. Immunoblots of conditioned media and supernatants of brain lysates were probed by anti-hsAPPα or anti-sAPPβ antibody. sAPPα or sAPPβ derived from both exogenous APP695 and endogenous APP770/751 are detected by each antibody. The increase in sAPPα by α-secretase activator and the reduction in sAPPα by α-secretase inhibitor effectively reached 434% and 50% of control (DMSO), respectively (upper panel). The decrease in sAPPβ by β-secretase inhibitor effectively reached 11% of control (lower panel). Neither sAPPα nor sAPPβ in the APP-KO brain was detected by anti-hsAPPα or anti-sAPPβ antibody, respectively. An asterisk indicates a non-specific band.
(TIF)

Figure S4 Immunocytochemical characterization of human ES cell (H9)-derived neuronal cells. (A) Time-dependent morphological changes of cells reseeded in a 24-well plate. Neuronal and glial cells were stained by anti-Tuj1 (left; red), anti-synapsin I (left; green), anti-MAP2 (right; red), and anti-GFAP (right; green) antibodies and DAPI (right; blue) at 38, 45, and 52 days. Scale bar, left; 20 μm, right; 50 μm. (B) ICC staining of Tbr1-, Ctip2-, Cux1- and Satb2-positive cells at day 52. (C–E) Neurotransmitter phenotypes at day 52. PAG (red)- and GAD (green)-positive (C), Glut1 (green)- and Tuj1 (red)-positive (D), and GABA (green)- and Tuj1 (red)-positive cells (E). Blue, DAPI. Scale bar, 50 μm.
(TIF)

Figure S5 Aβ production was modulated by several drugs in human ES cell-derived neuronal cells. β-Secretase inhibitor (BSI) (A, B), γ-secretase inhibitor (GSI) (C, D), and NSAID (E, F) were added into hES cell-derived neuronal cell cultures at day 36 (dotted line) and 50 (bold line), and two days later amounts of Aβ40 and Aβ42 secreted into the conditioned media were measured. The ratios Aβ40/FL-APP and Aβ42/FL-APP are expressed as percentages of the vehicle-treated group at day 52 and represent mean ± SD of 3 assays. *, $^{\#}p<0.05$, **, $^{\#\#}p<0.01$, ***, $^{\#\#\#}p<0.001$, significantly different from respective vehicle-treated groups by Dunnett's test.
(TIF)

Figure S6 Expression levels of reprogramming factors of iPS cells in neural differentiation. Total and transgene (Tg) expression levels of Sox2, Oct3/4 and Klf4 were measured by qPCR. Bold and dotted lines represent total and transgene expressions, respectively. "Fold expression" represents the ratio of the expression level compared to the total expression level at day 0 (iPS cells).
(TIF)

Figure S7 Aβ production was modulated by GSI in human iPS cell (201B7)-derived neuronal cells. γ-Secretase inhibitor (GSI) was added into the hiPS cell line, 201B7-derived neuronal cell cultures at day 36 (dotted line) and 50 (bold line), and two days later amounts of Aβ40 (A) and Aβ42 (B) secreted into the conditioned media were measured. The ratios Aβ40/FL-APP and Aβ42/FL-APP are expressed as percentages of the vehicle-treated group at day 52 and represent mean ± SD of 3 assays.
(TIF)

Protocol S1 Sampling method for checking antibody specificity.
(PDF)

Table S1 Effects of secretion inhibitors on cell viability measured by LDH assay at day 52.
(DOCX)

Table S2 qPCR primers.
(DOCX)

Acknowledgments

We would like to express our sincere gratitude to all our coworkers and collaborators, especially to K. Watanabe (RIKEN Brain Science Institute & Nagasaki University) for technical assistance and to K. Murai (CiRA) for editing manuscript.

Author Contributions

Conceived and designed the experiments: NI HI NY MA. Performed the experiments: NY MA NI. Analyzed the data: NY MA NI HI. Contributed reagents/materials/analysis tools: SK KT IA HH TK KM TCS TN TA SY. Wrote the paper: NY MA SY NI HI.

References

1. Selkoe DJ (2002) Alzheimer's disease is a synaptic failure. Science 298: 789–791.
2. Iwata N, Higuchi M, Saido TC (2005) Metabolism of amyloid-β peptide and Alzheimer's disease. Pharmacol Ther 108: 129–148.
3. Kukar TL, Ladd TB, Bann MA, Fraering PC, Narlawar R, et al. (2008) Substrate-targeting γ-secretase modulators. Nature 453: 925–929.
4. Kounnas MZ, Danks AM, Cheng S, Tyree C, Ackerman E, et al. (2010) Modulation of γ-secretase reduces β-amyloid deposition in a transgenic mouse model of Alzheimer's disease. Neuron 67: 769–780.
5. Takahashi K, Tanabe K, Ohnuki M, Narita M, Ichisaka T, et al. (2007) Induction of pluripotent stem cells from adult human fibroblasts by defined factors. Cell 131: 861–872.
6. Yu J, Vodyanik MA, Smuga-Otto K, Antosiewicz-Bourget J, Frane JL, et al. (2007) Induced pluripotent stem cell lines derived from human somatic cells. Science 318: 1917–1920.
7. Watanabe K, Kamiya D, Nishiyama A, Katayama T, Nozaki S, et al. (2005) Directed differentiation of telencephalic precursors from embryonic stem cells. Nat Neurosci 8: 288–296.
8. Gaspard N, Bouschet T, Hourez R, Dimidschstein J, Naeije G, et al. (2008) An intrinsic mechanism of corticogenesis from embryonic stem cells. Nature 455: 351–357.
9. Eiraku M, Watanabe K, Matsuo-Takasaki M, Kawada M, Yonemura S, et al. (2008) Self-organized formation of polarized cortical tissues from ESCs and its active manipulation by extrinsic signals. Cell Stem Cell 3: 519–532.
10. Li XJ, Zhang X, Johnson MA, Wang ZB, Lavaute T, et al. (2009) Coordination of sonic hedgehog and Wnt signaling determines ventral and dorsal telencephalic neuron types from human embryonic stem cells. Development 136: 4055–4063.
11. Zeng H, Guo M, Martins-Taylor K, Wang X, Zhang Z, et al. (2010) Specification of region-specific neurons including forebrain glutamatergic neurons from human induced pluripotent stem cells. PLoS One 5: e11853.
12. Chambers SM, Fasano CA, Papapetrou EP, Tomishima M, Sadelain M, et al. (2009) Highly efficient neural conversion of human ES and iPS cells by dual inhibition of SMAD signaling. Nat Biotechnol 27: 275–280.
13. Braak H, Braak E (1991) Neuropathological stageing of Alzheimer-related changes. Acta Neuropathol 82: 239–259.
14. Nakagawa M, Koyanagi M, Tanabe K, Takahashi K, Ichisaka T, et al. (2008) Generation of induced pluripotent stem cells without Myc from mouse and human fibroblasts. Nat Biotechnol 26: 101–106.
15. Wada T, Honda M, Minami I, Tooi N, Amagai Y, et al. (2009) Highly efficient differentiation and enrichment of spinal motor neurons derived from human and monkey embryonic stem cells. PLoS One 4: e6722.
16. Saito T, Hanai S, Takashima S, Nakagawa E, Okazaki S, et al. (2011) Neocortical layer formation of human developing brains and lissencephalies: consideration of layer-specific marker expression. Cereb Cortex 21: 588–596.
17. Kim JE, O'Sullivan ML, Sanchez CA, Hwang M, Israel MA, et al. (2011) Investigating synapse formation and function using human pluripotent stem cell-derived neurons. Proc Natl Acad Sci U S A 108: 3005–3010.
18. Akiyama H, Kaneko T, Mizuno N, McGeer PL (1990) Distribution of phosphate-activated glutaminase in the human cerebral cortex. J Comp Neurol 297: 239–252.
19. Blennow K, de Leon MJ, Zetterberg H (2006) Alzheimer's disease. Lancet 368: 387–403.
20. Kitazume S, Tachida Y, Kato M, Yamaguchi Y, Honda T, et al. (2010) Brain endothelial cells produce amyloid β from amyloid precursor protein 770 and preferentially secrete the O-glycosylated form. J Biol Chem 285: 40097–40103.
21. Yang LB, Lindholm K, Yan R, Citron M, Xia W, et al. (2003) Elevated β-secretase expression and enzymatic activity detected in sporadic Alzheimer disease. Nat Med 9: 3–4.
22. O'Connor T, Sadleir KR, Maus E, Velliquette RA, Zhao J, et al. (2008) Phosphorylation of the translation initiation factor eIF2α increases BACE1 levels and promotes amyloidogenesis. Neuron 60: 988–1009.
23. Parks AL, Curtis D (2007) Presenilin diversifies its portfolio. Trends Genet 23: 140–150.
24. Serneels L, Van Biervliet J, Craessaerts K, Dejaegere T, Horré K, et al. (2009) γ-Secretase heterogeneity in the Aph1 subunit: relevance for Alzheimer's disease. Science 324: 639–642.
25. McGowan E, Pickford F, Kim J, Onstead L, Eriksen J, et al. (2005) Aβ42 is essential for parenchymal and vascular amyloid deposition in mice. Neuron 47: 191–199.
26. Ono K, Condron MM, Ho L, Wang J, Zhao W, et al. (2008) Effects of grape seed-derived polyphenols on amyloid β-protein self-assembly and cytotoxicity. J Biol Chem 283: 32176–32187.
27. Hsiao K, Chapman P, Nilsen S, Eckman C, Harigaya Y, et al. (1996) Correlative memory deficits, Aβ elevation, and amyloid plaques in transgenic mice. Science 274: 99–102.
28. Kawarabayashi T, Younkin LH, Saido TC, Shoji M, Ashe KH, et al. (2001) Age-dependent changes in brain, CSF, and plasma amyloid β protein in the Tg2576 transgenic mouse model of Alzheimer's disease. J Neurosci 21: 372–381.
29. Mehta PD, Pirttilä T, Mehta SP, Sersen EA, Aisen PS, et al. (2000) Plasma and cerebrospinal fluid levels of amyloid β proteins 1-40 and 1-42 in Alzheimer disease. Arch Neurol 57: 100–105.
30. Asai M, Iwata N, Tomita T, Iwatsubo T, Ishiura S, et al. (2010) Efficient four-drug cocktail therapy targeting amyloid-β peptide for Alzheimer's disease. J Neurosci Res 88: 3588–3597.
31. Stachel SJ, Coburn CA, Steele TG, Jones KG, Loutzenhiser EF, et al. (2004) Structure-based design of potent and selective cell-permeable inhibitors of human β-secretase (BACE-1). J Med Chem 47: 6447–6450.
32. Seiffert D, Bradley JD, Rominger CM, Rominger DH, Yang F, et al. (2000) Presenilin-1 and -2 are molecular targets for γ-secretase inhibitors. J Biol Chem 275: 34086–34091.
33. Weggen S, Eriksen JL, Das P, Sagi SA, Wang R, et al. (2001) A subset of NSAIDs lower amyloidogenic Aβ42 independently of cyclooxygenase activity. Nature 414: 212–216.
34. Eriksen JL, Sagi SA, Smith TE, Weggen S, Das P, et al. (2003) NSAIDs and enantiomers of flurbiprofen target γ-secretase and lower Aβ 42 in vivo. J Clin Invest 112: 440–449.
35. Burton CR, Meredith JE, Barten DM, Goldstein ME, Krause CM, et al. (2008) The amyloid-β rise and γ-secretase inhibitor potency depend on the level of substrate expression. J Biol Chem 283: 22992–23003.
36. Games D, Adams D, Alessandrini R, Barbour R, Berthelette P, et al. (1995) Alzheimer-type neuropathology in transgenic mice overexpressing V717F β-amyloid precursor protein. Nature 373: 523–527.
37. De Meyer G, Shapiro F, Vanderstichele H, Vanmechelen E, Engelborghs S, et al. (2010) Diagnosis-independent Alzheimer disease biomarker signature in cognitively normal elderly people. Arch Neurol 67: 949–956.
38. Inoue H, Yamanaka S (2011) The use of induced pluripotent stem cells in drug development. Clin Pharmacol Ther 89: 655–661.
39. Iwatsubo T, Saido TC, Mann DM, Lee VM, Trojanowski JQ (1996) Full-length amyloid-β (1-42(43)) and amino-terminally modified and truncated amyloid-β 42(43) deposit in diffuse plaques. Am J Pathol 149: 1823–1830.
40. Johnson MA, Weick JP, Pearce RA, Zhang SC (2007) Functional neural development from human embryonic stem cells: accelerated synaptic activity via astrocyte coculture. J Neurosci 27: 3069–3077.
41. Lazarov O, Lee M, Peterson DA, Sisodia SS (2002) Evidence that synaptically released β-amyloid accumulates as extracellular deposits in the hippocampus of transgenic mice. J Neurosci 22: 9785–9793.
42. Soba P, Eggert S, Wagner K, Zentgraf H, Siehl K, et al. (2005) Homo- and heterodimerization of APP family members promotes intercellular adhesion. EMBO J 24: 3624–3634.
43. Woo SM, Kim J, Han HW, Chae JI, Son MY, et al. (2009) Notch signaling is required for maintaining stem-cell features of neuroprogenitor cells derived from human embryonic stem cells. BMC Neurosci 10: 97.
44. Mangialasche F, Solomon A, Winblad B, Mecocci P, Kivipelto M (2010) Alzheimer's disease: clinical trials and drug development. Lancet Neurol 9: 702–716.
45. Qiang L, Fujita R, Yamashita T, Angulo S, Rhinn H, et al. (2011) Directed conversion of Alzheimer's disease patient skin fibroblasts into functional neurons. Cell 146: 359–371.
46. Kaneko T, Urade Y, Watanabe Y, Mizuno N (1987) Production, characterization, and immunohistochemical application of monoclonal antibodies to glutaminase purified from rat brain. J Neurosci 7: 302–309.
47. Saido TC, Nagao S, Shiramine M, Tsukaguchi M, Sorimachi H, et al. (1992) Autolytic transition of mu-calpain upon activation as resolved by antibodies distinguishing between the pre- and post-autolysis forms. J Biochem 111: 81–86.

ARTHRITIS & RHEUMATISM
Vol. 63, No. 11, November 2011, pp 3625–3632
DOI 10.1002/art.30512

High Incidence of *NLRP3* Somatic Mosaicism in Patients With Chronic Infantile Neurologic, Cutaneous, Articular Syndrome

Results of an International Multicenter Collaborative Study

Naoko Tanaka,[1] Kazushi Izawa,[1] Megumu K. Saito,[2] Mio Sakuma,[3] Koichi Oshima,[4] Osamu Ohara,[4] Ryuta Nishikomori,[1] Takeshi Morimoto,[3] Naotomo Kambe,[5] Raphaela Goldbach-Mansky,[6] Ivona Aksentijevich,[6] Geneviève de Saint Basile,[7] Bénédicte Neven,[8] Mariëlle van Gijn,[9] Joost Frenkel,[9] Juan I. Aróstegui,[10] Jordi Yagüe,[10] Rosa Merino,[11] Mercedes Ibañez,[12] Alessandra Pontillo,[13] Hidetoshi Takada,[14] Tomoyuki Imagawa,[15] Tomoki Kawai,[1] Takahiro Yasumi,[1] Tatsutoshi Nakahata,[2] and Toshio Heike[1]

Objective. **Chronic infantile neurologic, cutaneous, articular (CINCA) syndrome, also known as neonatal-onset multisystem inflammatory disease (NOMID), is a dominantly inherited systemic autoinflammatory disease. Although heterozygous germline gain-of-function *NLRP3* mutations are a known cause of this disease, conventional genetic analyses fail to detect disease-causing mutations in ~40% of patients. Since somatic *NLRP3* mosaicism has been detected in several mutation-negative NOMID/CINCA syndrome patients, we undertook this study to determine the precise contribution of somatic *NLRP3* mosaicism to the etiology of NOMID/CINCA syndrome.**

Methods. **An international case–control study was performed to detect somatic *NLRP3* mosaicism in NOMID/CINCA syndrome patients who had shown no mutation during conventional sequencing. Subcloning and sequencing of *NLRP3* was performed in these mutation-negative NOMID/CINCA syndrome patients and their healthy relatives. Clinical features were analyzed to identify potential genotype–phenotype associations.**

Results. **Somatic *NLRP3* mosaicism was identified in 18 of the 26 patients (69.2%). Estimates of the level of mosaicism ranged from 4.2% to 35.8% (mean ± SD 12.1 ± 7.9%). Mosaicism was not detected in any of the 19 healthy relatives (18 of 26 patients versus 0 of 19**

Supported by Mitsubishi Pharma Research Foundation, the Japanese Ministry of Education, Science, Sports, and Culture, and the Japanese Ministry of Health, Labor, and Welfare.

[1]Naoko Tanaka, MD, Kazushi Izawa, MD, Ryuta Nishikomori, MD, PhD, Tomoki Kawai, MD, Takahiro Yasumi, MD, PhD, Toshio Heike, MD, PhD: Kyoto University Graduate School of Medicine, Kyoto, Japan; [2]Megumu K. Saito, MD, PhD, Tatsutoshi Nakahata, MD, PhD: Center for iPS Cell Research and Application, Kyoto, Japan; [3]Mio Sakuma, MD, PhD, Takeshi Morimoto, MD, PhD: Kyoto University, Kyoto, Japan; [4]Koichi Oshima, MD, Osamu Ohara, PhD: RIKEN Yokohama Institute, Yokohama, Kanagawa, and Kazusa DNA Research Institute, Kisarazu, Chiba, Japan; [5]Naotomo Kambe, MD, PhD: Chiba University Graduate School of Medicine, Chiba, Japan; [6]Raphaela Goldbach-Mansky, MD, Ivona Aksentijevich, MD: National Institute of Arthritis and Musculoskeletal and Skin Diseases, NIH, Bethesda, Maryland; [7]Geneviève de Saint Basile, MD, PhD: Paris Descartes University and INSERM U 768, Paris, France; [8]Bénédicte Neven, MD: Necker Hospital for Sick Children, AP-HP, Paris, France; [9]Mariëlle van Gijn, PhD, Joost Frenkel, MD, PhD: University Medical Centre Utrecht, Utrecht, The Netherlands; [10]Juan I. Aróstegui, MD, PhD, Jordi Yagüe, MD, PhD: Hospital Clínic, Barcelona, Spain; [11]Rosa Merino, MD, PhD: Hospital La Paz, Madrid, Spain; [12]Mercedes Ibañez, MD: Hospital Niño Jesús, Madrid, Spain; [13]Alessandra Pontillo, MD, PhD: IRCCS Burlo Garofalo, Trieste, Italy; [14]Hidetoshi Takada, MD, PhD: Kyushu University Graduate School of Medical Sciences, Fukuoka, Japan; [15]Tomoyuki Imagawa, MD, PhD:Yokohama City University School of Medicine, Yokohama, Kanagawa, Japan.

Drs. Tanaka and Izawa contributed equally to this work.

Dr. Goldbach-Mansky has served as an expert witness on behalf of Biovitrum, Novartis, and Regeneron.

Address correspondence to Osamu Ohara, PhD, Department of Human Genome Research, Kazusa DNA Research Institute, 2-6-7 Kazusakamatari Kisarazu, Chiba 292-0818, Japan (e-mail: ohara@kazusa.or.jp); or to Ryuta Nishikomori, MD, PhD, Department of Pediatrics, Kyoto University Graduate School of Medicine, 54 Shogoin Sakyo, Kyoto 606-8507, Japan (e-mail: rnishiko@kuhp.kyoto-u.ac.jp).

Submitted for publication March 10, 2011; accepted in revised form June 16, 2011.

relatives; $P < 0.0001$). In vitro functional assays indicated that the detected somatic *NLRP3* mutations had disease-causing functional effects. No differences in *NLRP3* mosaicism were detected between different cell lineages. Among nondescript clinical features, a lower incidence of mental retardation was noted in patients with somatic mosaicism. Genotype-matched comparison confirmed that patients with somatic *NLRP3* mosaicism presented with milder neurologic symptoms.

***Conclusion.* Somatic *NLRP3* mutations were identified in 69.2% of patients with mutation-negative NOMID/CINCA syndrome. This indicates that somatic *NLRP3* mosaicism is a major cause of NOMID/CINCA syndrome.**

Chronic infantile neurologic, cutaneous, articular (CINCA) syndrome (MIM no. #607715), also known as neonatal-onset multisystem inflammatory disease (NOMID), is a dominantly-inherited autoinflammatory disease that is characterized by neonatal onset and the triad of urticarial-like skin rash, neurologic manifestations, and arthritis/arthropathy. Patients often experience recurrent fever and systemic inflammation. NOMID/CINCA syndrome is the most severe clinical phenotype of the cryopyrin-associated periodic syndromes (CAPS) that also include the 2 less severe but phenotypically similar syndromes familial cold autoinflammatory syndrome (FCAS; MIM no. #120100) and Muckle-Wells syndrome (MIM no. #191900). CAPS are caused by mutations in the *NLRP3* gene, which is a member of the nucleotide-binding oligomerization domain–like receptor (NLR) family of the innate immune system (1,2).

NLRP3 is an intracellular "sensor" of danger signals arising from cellular insults, such as infection, tissue damage, and metabolic deregulation, and it has been highly conserved throughout evolution. NLRP3 associates with ASC and procaspase 1 to constitute a large multiprotein complex termed the NLRP3 inflammasome. When activated, the NLRP3 inflammasome converts the biologically inactive procaspase 1 into active caspase 1. Caspase 1 produces the cytokines interleukin-1β (IL-1β) and IL-18, which are mainly involved in the inflammatory response (3). Available research suggests that mutated *NLRP3* induces autoactivation of the NLRP3 inflammasome in CAPS patients, resulting in an uncontrolled overproduction of IL-1β.

Most CAPS patients carry heterozygous germline missense mutations in the *NLRP3* coding region ("mutation-positive" patients) (4,5). More than 80 different disease-causing mutations have been reported to date (6). However, ~40% of clinically diagnosed NOMID/CINCA syndrome patients show no heterozygous germline *NLRP3* mutation during conventional Sanger-sequencing-based genetic analyses ("mutation-negative" patients). Comparisons of NOMID/CINCA syndrome patients with and without heterozygous germline *NLRP3* mutations have revealed no differences in clinical features or response to treatment (4,7).

In a previous study, we identified a high incidence of somatic *NLRP3* mosaicism in "mutation-negative" NOMID/CINCA syndrome patients in Japan (8). We therefore hypothesized that somatic *NLRP3* mosaicism may be implicated in the etiology of the disorder, although its precise contribution remains unclear. The aim of the present study was to evaluate both the frequency of *NLRP3* somatic mosaicism in NOMID/CINCA syndrome patients and the association between somatic mosaicism and clinical phenotype using an international cohort of mutation-negative NOMID/CINCA syndrome patients.

PATIENTS AND METHODS

Study design and participants. International collaborators were contacted to identify mutation-negative NOMID/CINCA syndrome cases. A total of 20 DNA samples were received from 4 centers: France (n = 6), The Netherlands (n = 4), Spain (n = 3), and the US (n = 7). DNA samples had been extracted from peripheral blood mononuclear cells or whole blood. All 20 samples had been subjected to conventional sequencing, and no *NLRP3* mutations had been identified. In each case, the accuracy of the clinical diagnosis had been confirmed according to the diagnostic criteria (7). The 6 previously reported Japanese cases and 1 Spanish case with *NLRP3* somatic mosaicism were also included (8,9). DNA samples were also collected from 19 healthy relatives of 8 patients (8 from France, 5 from Japan, 2 from Spain, and 4 from the US) to evaluate the causality of somatic *NLRP3* mosaicism in a case–control manner, since the clinical features may be modified by genetic and environmental factors.

Written informed consent for *NLRP3* gene analysis was obtained from all patients and controls. The study was approved by the Institutional Review Board of the Kyoto University Graduate School of Medicine and was conducted in accordance with the Declaration of Helsinki.

Data collection. *Demographic and clinical data.* The clinicians responsible for each mutation-negative NOMID/CINCA syndrome patient completed a questionnaire to document characteristics such as age, sex, race, symptoms, clinical findings, clinical course, and prognosis. No clinical data were obtained from the healthy controls.

Investigation of NLRP3 gene mosaicism. Disease-causing mutations in NOMID/CINCA syndrome patients have

only been reported in exons 3, 4, and 6 of *NLRP3* (6). Thus, the present sequencing was focused on a search for somatic mosaicism of these 3 exons and their flanking intronic regions. After amplifying these genomic regions with the proofreading polymerase chain reaction (PCR) enzyme KOD-Plus polymerase (Toyobo) and dA addition with an LA *Taq* polymerase (Takara Bio), the amplicons were subcloned into pCR2.1-TOPO vector (Invitrogen). Ninety-six clones were selected at random for each amplicon. The subcloned amplicons were retrieved by PCR with LA *Taq* polymerase. They were then treated with ExoSAP-IT (USB) and proteinase K (Promega) prior to direct sequencing. The cloned exons were sequenced at the Kazusa DNA Research Institute using a BigDye Terminator kit (version 3.1) and an ABI 3730 DNA sequencer (Life Technologies). Mosaicism was indicated by the detection of >2 subclones carrying the same base variation at the same position in 96 clones.

To purify leukocyte subpopulations, freshly drawn whole blood was separated using sequential dextran and Ficoll-Hypaque density-gradient centrifugation methods. Cell sorting to select T cells, B cells, and monocytes was performed with an AutoMACS Pro Separator (Miltenyi Biotec) or a FACSVantage System (BD Biosciences), as described elsewhere (8,9). The purity of each cell lineage was >90%. The level of mosaicism was determined by sequencing each source of genomic DNA from 80 clones.

Plasmids and cell lines. To determine whether the identified NLRP3 mutants cause disease, experiments for assessing 2 pathologic functions were performed as described elsewhere (8). Briefly, ASC-dependent NF-κB activation was performed by a dual-luciferase reporter assay in HEK 293FT cells transfected with NLRP3 mutants. Transfection-induced cell death in the human monocytic cell line THP-1 was performed by transfecting green fluorescent protein–fused mutant NLRP3 into THP-1 cells and then measuring the dead cells with 7-aminoactinomycin D.

Statistical analysis. The study was designed to detect mosaicism at a 5% allele frequency with >95% possibility. To satisfy this condition, it was necessary to sequence at least 93 clones per patient. The following calculation was used to estimate the number of clones that had to be sequenced: $P = 1 - (1 - 0.05)^n - n(0.05)(1 - 0.05)^{n-1}$ ($n = 93$, $P = 0.956$). The study was designed to analyze 96 PCR-fragment clones from each patient. The error rate of the PCR reactions was estimated using a proofreading KOD-Plus enzyme. We analyzed a plasmid vector carrying a normal *NLRP3* exon 3, in which 2 distinct errors were detected by sequencing 91 clones. The calculated error rate for this result was 1/87,451 (2/[1,922 bp × 91 clones]). Thus, the probability was negligible that the same errors would be detected more than twice in 96 clones from 1 patient.

To calculate the sample size, we calculated the prevalence of somatic mosaicism among mutation-negative NOMID/CINCA syndrome patients. Eight cases of somatic mosaicism were identified among 15 mutation-negative NOMID/CINCA syndrome patients who were subsequently analyzed by the subcloning method described above. It was assumed that the maximum number of possible somatic mosaicism cases among family controls was 1. On the basis of these data and this assumption, it was calculated that 19 controls were required to ensure a 2-sided alpha level of 0.05 and a power of 0.8.

Continuous variables are presented as the mean ± SD or as the median and interquartile range. Categorical variables are presented as numbers and ratios (with percentages). To compare clinical data between patients with and patients without mosaicism, the Wilcoxon rank sum test was used for continuous variables and Fisher's exact test was used for categorical variables. Fisher's exact test was used to compare the difference in mosaicism ratio between cases and controls. The chi-square test was used to compare the difference in the level of mosaicism between different sources of genomic DNA from each patient.

Table 1. Somatic mosaicism among mutation-negative NOMID/CINCA syndrome patients*

Country, patient	Sequence variant	Protein variant	Mosaicism, %
France			
F1	1298C>T	T433I	5.2
F2	907G>C	D303H	4.2
F3	1315G>C	A439P	21.9
F4	1216A>G	M406V	9.2
F5	1698C>A	F566L	11.5
F6	None	–	–
Japan			
J1	1709A>G	Y570C	12.2
J2	790C>T	L264F	4.3
J3	919G>A	G307S	10.7
J4	1699G>A	E567K	6.5
J5	907G>C	D303H	11.9
J6	None	–	–
Spain			
S1	920G>T	G307V	9.6
S2	907G>C	D303H	19.1
S3	None	–	–
S4	None	–	–
US			
A1	1065A>T	K355N	18.8
A2	1698C>A	F566L	14.6
A3	1704G>C	K568N	9.4
A4	2263G>A	G755R	35.8
A5	None	–	–
A6	None	–	–
The Netherlands			
N1	1699G>A	E567K	6.3
N2	2263G>A	G755R	6.3
N3	None	–	–
N4	None	–	–

* *NLRP3* mosaicism was detected in 18 of 26 patients (69.2%) with neonatal-onset multisystem inflammatory disease (NOMID)/chronic infantile neurologic, cutaneous, articular syndrome (CINCA syndrome). When samples from 19 healthy relatives of these patients were investigated, no somatic mosaicism was detected. The *P* value from the comparison of the cases and the controls (18 of 26 versus 0 of 19) was statistically significant ($P < 0.0001$).